iScience

CellPress

Article

Ex Vivo/In vivo Gene Editing in Hepatocytes Using "All-in-One" CRISPR-Adeno-Associated Virus Vectors with a Self-Linearizing Repair Template

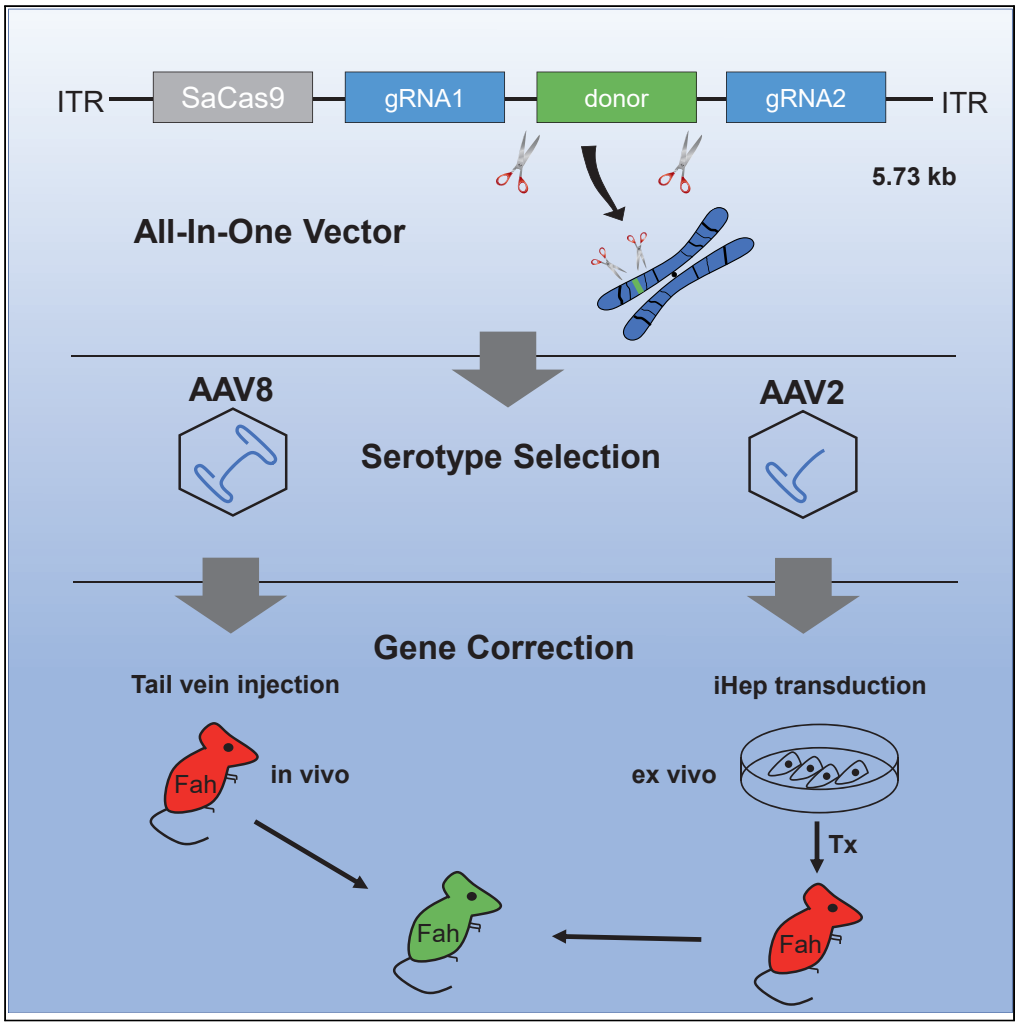

Simon Alexander Krooss, Zhen Dai, Florian Schmidt, ..., Amar Deep Sharma, Hildegard Büning, Michael Ott

ott.michael@mh-hannover.de, ott-mhh@gmx.de

HIGHLIGHTS

Single AAV vector mediates efficient large fragment replacement *in vivo* and *ex vivo*

Fah-corrected iHeps repopulate the liver of recipient mice

Self-linearizing donor template enhances integration rate

AAV2 and AAV8 reveal differences in packaging the oversized AIO-SL vector genome

Krooss et al., iScience *23*, 100764
January 24, 2020
https://doi.org/10.1016/j.isci.2019.100764

iScience

CellPress

Article

Ex Vivo/In vivo Gene Editing in Hepatocytes Using "All-in-One" CRISPR-Adeno-Associated Virus Vectors with a Self-Linearizing Repair Template

Simon Alexander Krooss,[1,2,5,11] Zhen Dai,[1,3,11] Florian Schmidt,[6,7,10] Alice Rovai,[1,2] Julia Fakhiri,[6,8] Akshay Dhingra,[5] Qinggong Yuan,[1,2] Taihua Yang,[3] Asha Balakrishnan,[1,2] Lars Steinbrück,[5] Sangar Srivaratharajan,[5] Michael Peter Manns,[1] Axel Schambach,[4] Dirk Grimm,[6,7,8] Jens Bohne,[5] Amar Deep Sharma,[1,3,11] Hildegard Büning,[4,9,11] and Michael Ott[1,2,11,12,*]

SUMMARY

Adeno-associated virus (AAV)-based vectors are considered efficient and safe gene delivery systems in gene therapy. We combined two guide RNA genes, Cas9, and a self-linearizing repair template in one vector (AIO-SL) to correct fumarylacetoacetate hydrolase (FAH) deficiency in mice. The vector genome of 5.73 kb was packaged into VP2-depleted AAV particles (AAV2/8$^{\Delta VP2}$), which, however, did not improve cargo capacity. Reprogrammed hepatocytes were treated with AIO-SL.AAV2$^{\Delta VP2}$ and subsequently transplanted, resulting in large clusters of FAH-positive hepatocytes. Direct injection of AIO-SL.AAV8$^{\Delta VP2}$ likewise led to FAH expression and long-term survival. The AIO-SL vector achieved an ~6-fold higher degree of template integration than vectors without template self-linearization. Subsequent analysis revealed that AAV8 particles, in contrast to AAV2, incorporate oversized genomes distinctly greater than 5.2 kb. Finally, our AAV8-based vector represents a promising tool for gene editing strategies to correct monogenic liver diseases requiring (large) fragment removal and/or simultaneous sequence replacement.

INTRODUCTION

CRISPR-associated protein 9 (Cas9) is an RNA-guided DNA endonuclease associated with the clustered regularly interspaced short palindromic repeats (CRISPR) machinery and has been adapted to induce site-directed double-strand breaks (DSBs) into DNA (Jinek et al., 2013). CRISPR/Cas9 technology has revolutionized the field of gene editing and is currently being developed for therapeutic purposes in many organs and species. Gene modification by CRISPR/Cas9 after DNA DSBs may either be achieved by non-homologous end joining (NHEJ) or by homology-directed repair (HDR) through incorporation of an ectopic gene template.

The liver is a preferred organ for cell and gene therapy as well as gene editing, because hereditary diseases are numerous and often life-threatening. HDR in tyrosinemia mice as model organism has been demonstrated to correct the disease, although the efficiency of homologous recombination without induction of DSBs was very low (Paulk et al., 2010; Junge et al., 2018). In a similar mouse model, a CRISPR/Cas9-mediated phenotype rescue was demonstrated via hydrodynamic DNA injection (Yin et al., 2014) and a combination of non-viral Cas9 mRNA with adeno-associated viral (AAV) vector-mediated HDR template delivery (Yin et al., 2016). AAV vectors have emerged as gene delivery vehicles for the liver with reports of impressive therapeutic efficacies in human clinical trials (Nathwani et al., 2014). Recently, the administration of a dual AAV vector system coding for a *Streptococcus pyogenes* Cas9 (SpCas9) expression cassette on one vector, and guide RNA (gRNA) and repair template on a second vector, reversed a mutation in the ornithine transcarbamylase gene in newborn mice (Yang et al., 2016). The segmentation of this *in vivo* gene editing tool on two vectors is owed to the proposed packaging size limitation of AAV, which is 4.9 kb (Grieger and Samulski, 2005) to 5 kb (Wu et al., 2010). Co-delivery of two different AAV vectors each encoding parts of the required components, which are reunited within the cells by *trans*-splicing, homologous recombination, or inteins (Truong et al., 2015), is feasible but occurs *in vivo* at low rates (Xu et al., 2004).

Here, we constructed a single AAV vector coding for Cas9, a repair template, and two gRNA genes resulting in a vector genome of 5.73 kb (excluding inverted terminal repeats [ITRs]) to correct the

Continued

[1]Department of Gastroenterology, Hepatology and Endocrinology, Hannover Medical School, Hannover, Germany

[2]Twincore Centre for Experimental and Clinical Infection Research, Hannover, Germany

[3]Junior Research Group MicroRNA in Liver Regeneration, Cluster of Excellence REBIRTH, Hannover Medical School, Hannover, Germany

[4]Institute for Experimental Hematology, Cluster of Excellence REBIRTH, Hannover Medical School, Hannover, Germany

[5]Institute for Virology, Hannover Medical School, Hannover, Germany

[6]Bioquant, University of Heidelberg, Heidelberg, Germany

[7]German Center for Infection Research (DZIF), and German Center for Cardiovascular Research (DZHK), Partner Site Heidelberg, Hannover, Germany

[8]Center for Infectious Diseases/Virology, Cluster of Excellence Cell Networks, Heidelberg University Hospital, Heidelberg, Germany

[9]German Center for Infection Research (DZIF), Partner Site Hannover-Braunschweig, Hannover, Germany

[10]Present address: Department of Biosystems Science and Engineering, ETH Zürich, Basel, Switzerland

fumarylacetoacetate hydrolase (Fah) exon 5 in a tyrosinemia mouse model (Grompe et al., 1993). The vector was packaged into an AAV variant devoid of the minor capsid protein VP2 (ΔVP2). The decision was based on the fact that VP2 is non-essential for assembly and infectivity (Warrington et al., 2004), but requires space in the capsid as the N-terminal domain of the five VP2 proteins is orientated to the inside of the capsid (Bleker et al., 2006). Grieger and Samulski (Grieger and Samulski, 2005) tested this strategy in the past for serotypes 1–5 without observing benefit regarding packaging capacity. Albeit no improvement was detected in their study, we decided to test this strategy particularly in the context of AAV8 as its hepatotropism represents an attractive advantage for the purpose of our study and, generally, the efficient delivery of oversized transgenes via AAV to the liver remains a desirable tool. The donor template was flanked by the genomic sequences to be targeted by SaCas9 to allow excision before homologous recombination. The viral vector was employed in $Fah^{-/-}$ transcription-factor-reprogrammed hepatocytes *ex vivo*, which were then transplanted, as well as directly *in vivo* by tail vein injection. Both approaches resulted in successful liver repopulation by Fah-corrected hepatocytes and long-term survival without 2-(2-nitro-4-trifluormethyl-benzoyl)-1,3-cyclohexandion (NTBC), which blocks the tyrosine catabolism pathway further upstream avoiding accumulation of fumarylacetoacetate. Subsequent analysis revealed that, albeit $AAV8\Delta^{VP2}$ vector particles demonstrated efficient gene correction capacity, deletion of VP2 did not increase the packaging capacity. In line with Grieger and Samulski, we also did not observe an advantage for AAV2. However, when comparing the natural packaging capacity of AAV8 and AAV2 capsids with or without VP deletion, we surprisingly observed an obvious difference. Specifically, AAV8 vectors packaged genomes of up to 6.17 kb, whereas AAV2 vectors reached, in line with literature, the threshold at approximately 5 kb.

RESULTS

CRISPR/SaCas9 Precisely Excises neoR in C57BL/6 *Fah*$^{\Delta exon5}$ MEFs

In the C57BL/6 *Fah*$^{\Delta exon5}$ tyrosinemia type 1 disease mouse model published originally by Grompe and colleagues (Grompe et al., 1993), a neomycin resistance (neoR) cassette disrupts the Fah exon 5 sequence as shown in Figure 1A. As a result, these mice depend on lifelong NTBC administration to circumvent fumarylacetoacetate accumulation due to Fah deficiency. To reconstitute the gene via integration of a donor template, prior removal of the resistance sequence via two simultaneous DSBs in DNA is required. Consequently, two SaCas9-compatible gRNAs were designed to target the neoR sequence, gRNA1 and gRNA2. The removal of the neoR sequence by SaCas9 guided by these two gRNAs would lead to exon 5 lacking 5 nucleotides and incorporating 12 nucleotides of the resistance cassette (Figures 1A and 1B (iii)). Owing to insertion of the resistance cassette, the Fah exon 5 lacks four nucleotides compared with the wild-type as indicated in Figure 1B (ii). Co-transfection of gRNA1 and gRNA2 together with SaCas9 into $Fah^{-/-}$ mouse embryonic fibroblasts (MEFs) led to perfect removal of the intervening sequence via simultaneous DSBs, as confirmed by PCR showing a product of ~200 bp matching the wild-type sample (Figure 1C).

NHEJ represents a preferred pathway in the repair of DNA DSBs, which is responsible for the formation of insertions and deletions (indels) (Bassing and Alt, 2004). Interestingly, subcloning and sequencing of the band highlighted in Figure 1C indicates indel-free repair in 77.5% of the clones analyzed (n = 40) and indel formation in 22.5% (Figure 1D). The religation junction of the two exon 5 strands after perfect DSB repair is depicted in Figure 1E.

Vector Architecture and Deletion of the VP2 Domain

To generate an alternative to a dual vector system, we combined all components required for neoR excision and Fah exon 5 replacement on a single molecule. Specifically, we cloned a single-stranded (ss)AAV vector harboring an LP1 (Nathwani et al., 2014) (liver promoter 1) promoter-driven SaCas9 followed by the bGH poly(A) signal, two gRNA expression cassettes, and a donor template devoid of the PAM (protospacer adjacent motif) of gRNA1. Arms of homology of 200 bp each flank the Fah exon 5 sequence. In addition, the donor template was flanked with the sequences to be targeted in the genome including the corresponding PAMs, orientated toward the donor template (Figure 2A). As this step facilitates intranuclear self-linearization of the donor template, we hypothesized that this event may increase the availability of the donor template for genomic integration. Indeed, it has previously been reported that an *in vivo* linearization of a donor transgene by zinc-finger nucleases led to increased numbers of integration events at different genomic loci (Cristea et al., 2013). Here, we employed the strategy of self-linearization with another nuclease delivered by AAV.

[11]These authors contributed equally

[12]Lead Contact

*Correspondence: ott.michael@mh-hannover.de, ott-mhh@gmx.de

https://doi.org/10.1016/j.isci.2019.100764

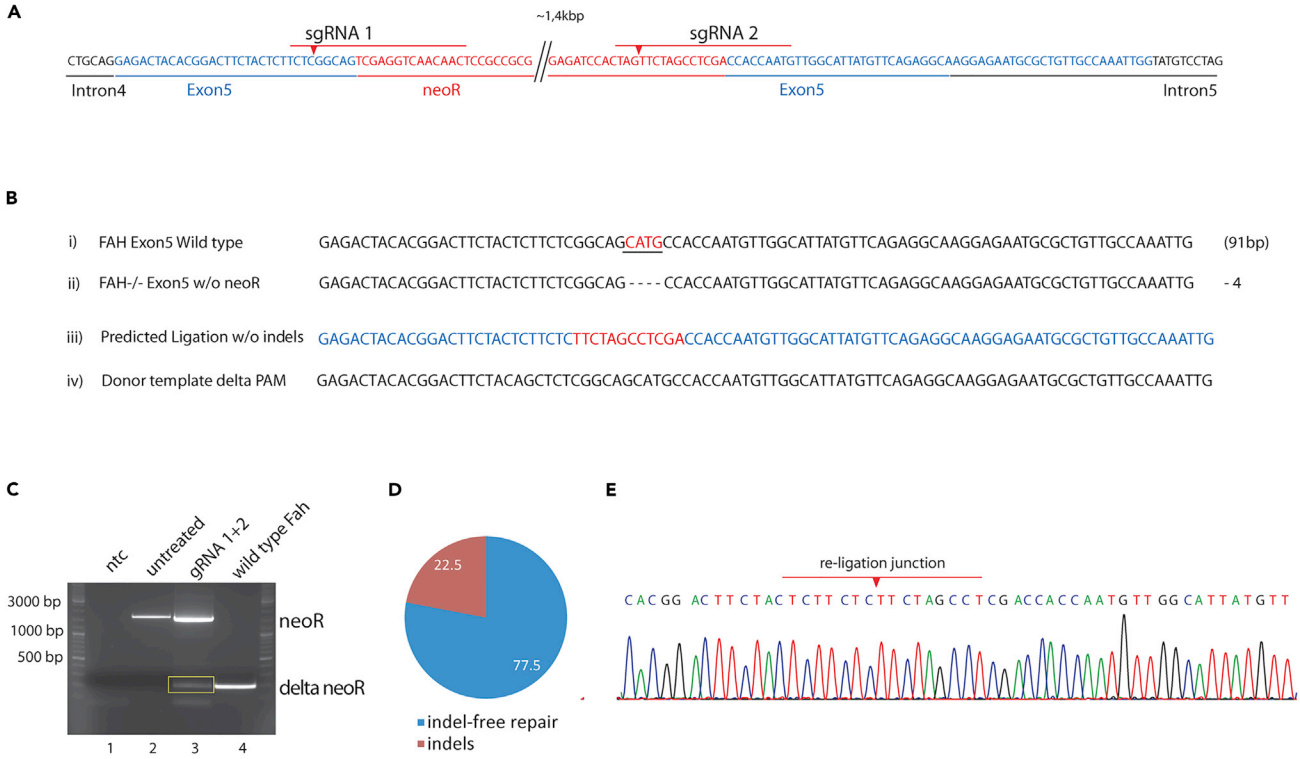

Figure 1. Excision of neoR Sequence via Two Simultaneous DSBs

(A) Fah exon 5 present in the genome of C57BL/6 *Fah*$^{\Delta exon5}$mice. Exon 5 (blue) is disrupted by the insertion of a ~1.4-kb neoR sequence (red). Sequencing results revealed the absence of four nucleotides due to the insertion of neoR. Target regions of gRNA1 and 2 are indicated by red lines, and predicted cleavage positions are denoted by a spike.

(B) Sequence of the wild-type murine Fah exon 5. The four lacking nucleotides due to neoR insertion are highlighted in red. Second row shows the hypothetical sequence of Fah exon 5 after removal of neoR. The third row represents Fah exon 5 after Cas9-mediated excision of neoR using gRNA1 and gRNA2. NeoR remnants are highlighted in red. The donor template used in subsequent experiments is depicted in the fourth row. The PAM of gRNA1 is degenerated by silent mutations.

(C) Fah$^{-/-}$ MEFs were co-transfected with SaCas9, gRNA1 and gRNA2. Genomic DNA was isolated and analyzed by PCR using P16/P11. The ~1.5-kb band (lane 2 and 3) represents a PCR product of Fah exon 5 incorporating neoR, whereas the 200-bp band (lanes 3 and 4) refers to the authentic length of Fah exon 5. Wild-type genomic DNA served as a template representing the positive control (lane 4).

(D) The PCR product highlighted in yellow in (C) was purified and subcloned into a sequencing vector. Colonies (n = 40) were selected and analyzed by Sanger sequencing. The blue area (77.5%) represents sequencing results indicating indel-free repair; the red area (22.5%) represents indel-derived reads.

(E) Representative Sanger sequencing chromatogram of the indel-free religation junction as described in (D).

The overall length of the AIO-SL (all-in-one-self-linearizing) construct amounts to 5.73 kb (excluding the AAV ITRs, i.e., the ITRs that flank the transgene and that are essential for viral vector genome packaging into AAV capsids), thereby exceeding the wild-type AAV genome size by roughly 1 kb. As the N′-termini of AAV's minor capsid proteins, VP1 and VP2, are located within the capsid interior (Bleker et al., 2006) the assumption is obvious that packaging of larger genomes becomes possible if AAV capsids devoid of the non-essential VP2 capsid proteins are used for vector production. However, Grieger and Samulski reported that at least for serotypes 1–5 this hypothesis does not hold true (Grieger and Samulski, 2005). As serotypes differ in their capsid features, we, despite the unsuccessful attempt of Grieger and Samulski, followed this hypothesis for AAV8 and used AAV2Δ^{VP2} as reference (Figure 2B). These serotypes were chosen, because AAV2 represents an attractive vehicle for cultured cells (Smith et al., 2004), such as our iHeps, and AAV8 is known for its hepatotropism (Nakai et al., 2005), but presents rather low transduction rates in primary cells (Ellis et al., 2013). The absence of the VP2 protein was confirmed by immunoblot using AAV8 preparations as example (Figure 2C). The wild-type AAV capsid preparation exhibits the expected approximately 1:1:10 stoichiometry of VP1, VP2, and VP3, whereas the ΔVP2 AAV capsid lacks the VP2 band.

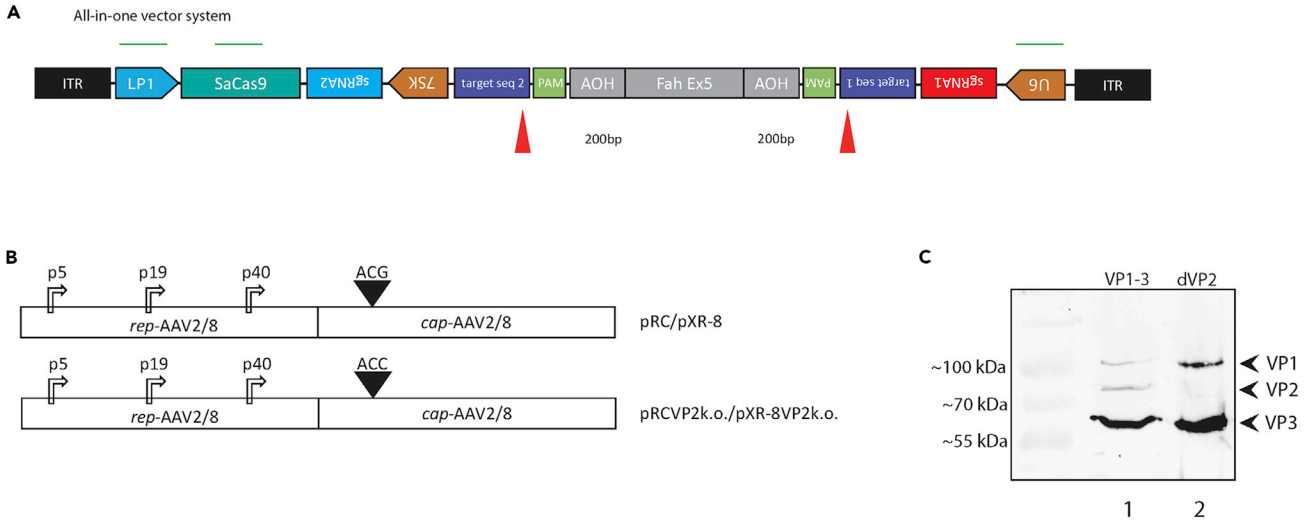

Figure 2. Vector Construction of AIO-SL and Capsid Modification

(A) Depiction of the AIO-SL vector architecture. The construct is flanked by ITRs. Target sequence 1/2 and PAM (indicated in purple and green, respectively) flank the donor template (gray). Spikes located at the flanks of the donor template in the AIO-SL vector symbolize the cleavage positions required for intracellular linearization of the donor template. Green lines indicate the position of the qPCR amplicons utilized for truncation analysis in Figure 6A.

(B) VP2 start codon mutagenesis within the *cap* open reading frame. The diagram shows the modification of pRC and pXR-8, resulting in pRCVP2k.o. or pXR-8VP2k.o.

(C) Detection of the AAV capsid proteins VP1, VP2, and VP3 in purified AAV8 capsids derived from either pXR-8 (lane 1, VP1-3) or pXR-8VP2k.o (lane 2, VP2k.o.).

Determination of Editing Efficiency

To evaluate whether our vector comprising a self-linearizing donor template as shown in Figures 2A and 3A (i) has an advantage over a vector lacking this feature, we constructed an appropriate non-self-linearizing control, referred to as AIO-NL (Figure 3A (ii)). This vector is devoid of the genomic target sequences at the flanks of the donor template and the corresponding PAMs. Otherwise, the construct is identical to AIO-SL (Figure 3A (i)). To compare the two AIO vectors with a regular size system, we separated the LP1 promoter-driven SaCas9 from the two gRNA cassettes and the donor template, thereby generating a dual vector system (DV) based on two ssAAV (Figure 3A (iii)). Furthermore a vector devoid of SaCas9, referred to as noCas9 (Figure 3A (iv)), was constructed to investigate whether the donor template itself could reconstitute the Fah open reading frame.

As the integration of the donor template requires substitution of the neoR cassette, we assessed editing efficiency by measuring the abundance of neoR sequences via qPCR in genomic DNA of $Fah^{-/-}$ MEFs transduced with noCas9.AAV2^{VP1-3} DV.AAV2^{VP1-3} AIO-SL.AAV2$^{\Delta VP2}$ and AIO-NL.AAV2$^{\Delta VP2}$ particles delivering the above-mentioned genomes (Figure 3B). This qPCR strategy allows for the identification and quantification of genomes lacking neoR, indicative of successful removal via simultaneous DSBs. Furthermore, it avoids false-positive results that could be generated by an Fah exon 5-specific amplicon derived from the donor template. Genome editing events were detectable after transduction at multiplicity of infection (MOI), i.e., vector genome containing particles (vg) per cell, of 5×10^5. Both, AIO-SL and AIO-NL led to a reduction of neoR abundance (77.85% ± 6.46% and 76.11% ± 4.03%) comparable to the DV (74.63% ± 12.8%). Importantly, the noCas9-AAV2-treated $Fah^{-/-}$ MEFs exhibited no distinct reduction of neoR (Figure 3B), indicating that nuclease activity is required for the removal of neoR.

As both AIO vectors led to loss of neoR comparable to the DV, we proceeded with the AIO-SL and AIO-NL vectors for further experiments (Figure 3C, blue area). To determine the frequency of donor integration events upon neoR excision, next-generation sequencing (NGS) was performed on the PCR product generated by primers P11/P12 and shortened by primers P11/P17. This PCR strategy only amplifies Fah exon 5 sequences lacking neoR and avoids unintended amplification of donor templates derived from the viral vector genomes (Figure S1). NGS analysis via CRISPESSO (Pinello et al., 2016) revealed a donor integration rate of 9.15% ± 1.2% upon treatment with the AIO-NL vector versus 58.55% ± 3.29% upon AIO-SL

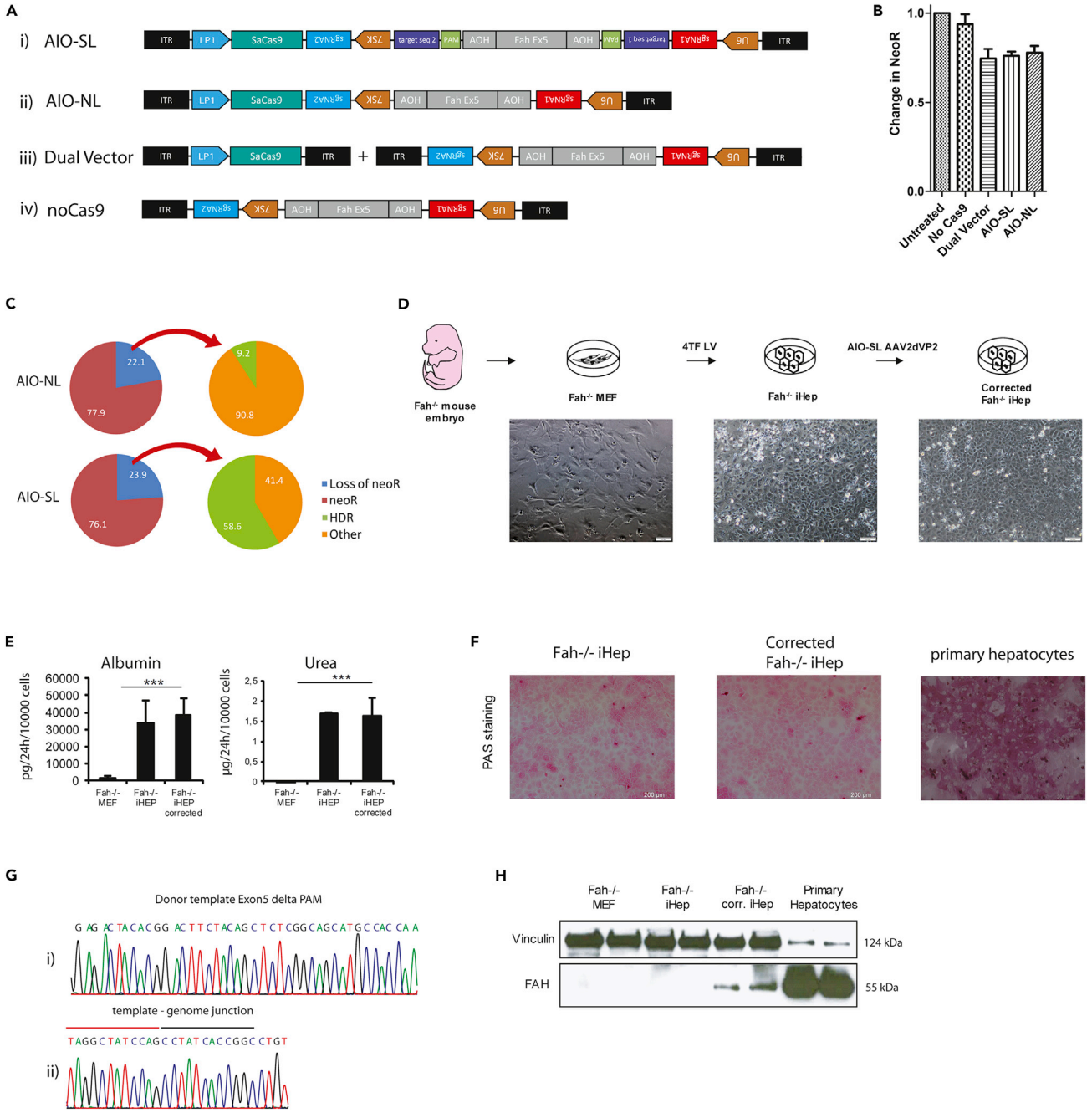

Figure 3. Analysis of Editing Efficiency and Direct Reprogramming of Fah$^{-/-}$ MEFs

(A) Vector architecture of (i) AIO-SL, (ii) AIO-NL, (iii) dual vector system, and (iv) noCas9.

(B) qPCR detecting the neoR sequence in genomic DNA of Fah$^{-/-}$ MEFs transduced (MOI 5×10^5) with noCas9_AAV2 (n = 4, SD = 12.6), DV_AAV2 (n = 4, SD = 12.8), AIO-SL.AAV2 $^{\Delta VP2}$ (n = 4, SD = 4.48), or AIO-NL.AAV2 $^{\Delta VP2}$ (n = 4, SD = 3.01).

(C) The blue/red pie chart depicts of loss-of-neoR ratios as determined in (B) from cells treated with AIO-SL.AAV2 $^{\Delta VP2}$ and AIO-NL.AAV2 $^{\Delta VP2}$ (loss of neomycin = 100 - neoR). The green/orange pie charts depict the percentage of donor integration reads (green) versus other repair (orange) determined via NGS. Genomic DNA of treated cells was subjected to PCR strategies depicted in Figure S1. AIO-SL.AAV2 $^{\Delta VP2}$-treated Fah$^{-/-}$ MEF show a donor integration rate of 58.55% ± 3.29% (n = 4), whereas AIO-NL.AAV2 $^{\Delta VP2}$-treated Fah$^{-/-}$ MEFs only had 9.15% ± 1.2% integration (n = 4).

(D) Experimental workflow. Following the isolation of MEFs from Fah$^{-/-}$ animals, they were reprogrammed into iHeps via lentiviral transduction of four transcription factors. Subsequently, the iHeps were transduced with AIO-SL.AAV2$^{\Delta VP2}$. Phase contrast microscopy of Fah$^{-/-}$ MEFs and Fah$^{-/-}$ iHep. Scale bar, 100 µm.

Figure 3. *Continued*

(E) Albumin secretion analyzed in untreated Fah$^{-/-}$ MEFs, iHeps, and AAV2-treated iHeps. (n = 4 biological replicates, $p < 0.01$ compared with MEFs, Student's t test). Urea secretion was analyzed in untreated Fah$^{-/-}$ MEFs, iHeps, and AAV2-treated iHeps (n = 4, $p < 0.01$).

(F) Periodic acid-Schiff staining in AAV2-treated and untreated Fah$^{-/-}$ iHeps. Scale bar, 200 μm.

(G) Sanger sequencing chromatogram depicting the detection of the donor template. The sequencing read reaches into the genome (template-genome junction indicated by red bar), thereby demonstrating integration of the donor template.

(H) Detection of FAH protein in Fah$^{-/-}$ MEFs, untreated Fah$^{-/-}$ iHeps, and corrected iHeps by immunoblotting. A cell lysate of primary hepatocytes serves as a positive control. Vinculin was used as a loading control.

treatment (values apply to the loss-of-neoR fraction) (Figure 3C, green/orange pie chart). Together with the data obtained from the loss-of-neoR qPCR, we can conclude that AIO-NL transduction led to a total knockin rate of ~2.18%, whereas AIO-SL-treated cells display a rate of ~13.24%. Owing to this remarkable ~6-fold increase in donor integration rate caused by vector self-linearization, all further experiments were conducted using the AIO-SL vector.

Direct Reprogramming of Fah-Deficient MEFs into iHeps and Subsequent Genome Editing Results in Fah Expression

Next, Fah$^{-/-}$ MEFs were directly reprogrammed into hepatocyte-like cells by lentiviral delivery of the four transcription factors FOXA3, GATA4, HNF1A, and HNF4A as previously published (Song et al., 2016). Subsequently, the cells were transduced with AIO-SL.AAV2$^{\Delta VP2}$. Reprogramming of Fah-deficient MEFs into iHeps could be observed by assessing cell morphology (Figure 3D) as well as functional properties, such as albumin and urea secretion. The latter clearly differed from the secretion levels of untreated MEFs, but were largely identical between AAV2$^{\Delta VP2}$ vector-treated iHeps and untreated iHeps (Figure 3E). Furthermore, metabolic functions such as indocyanine green uptake (data not shown) and glycogen synthesis of iHeps were not affected by vector treatment and genome editing (Figure 3F). Sanger sequencing of the neoR-deficient PCR product clearly confirms integration of the donor template (Figure 3G). qPCR analysis revealed a loss of neoR of 32.3% ± 6.8%, of which 74.7% showed integration of the donor template as determined by NGS, resulting in an overall knockin rate of approximately 24.1% (Figure S2). Next, we analyzed the extent of gene correction at the protein level. Upon AIO-SL.AAV2$^{\Delta VP2}$ treatment and genome editing, FAH protein was detected in iHeps by immunoblotting (Figure 3H), whereas Fah$^{-/-}$ MEFs and untreated Fah$^{-/-}$ iHeps showed no FAH protein expression.

Liver Repopulation and Long-Term Survival after Transplantation of Fah Gene-Corrected iHeps

We then tested whether re-expression of the FAH protein resulted in functionally competent cells in a liver repopulation assay. Following correction of the Fah reading frame and reconstitution of Fah expression *ex vivo*, the modified iHeps were transplanted into adult Fah-deficient recipient mice 14 days post-AIO-SL.AAV2$^{\Delta VP2}$ transduction (Figure 4A). Subsequent to the intrasplenic injection of 1×10^6 AIO-SL.AAV2$^{\Delta VP2}$-treated iHeps, NTBC was withdrawn and body weight of the animals was monitored. Forty days post-transplantation, the body weight of the treated animals had stabilized, whereas the general health of the control animals rapidly deteriorated after NTBC withdrawal (Figure 4B). Eight weeks after transplantation, liver samples were collected via partial hepatectomy and sections stained for FAH protein. Liver sections of transplanted animals showed robust repopulation by gene-corrected, FAH protein-expressing iHeps (Figure 4C). Neither neoplasias nor other abnormalities were observed in the treated animals, and aspartate and alanine aminotransferase levels were not elevated (data not shown). A cohort of animals that was followed for up to 7 months was also found to be tumor free. Normal hepatic histology was confirmed by H&E staining (Figure 4D). A secondary transplantation of iHeps obtained from a repopulated liver stabilized body weight of recipient animals and resulted in long-term survival (Figure S3).

Single Administration of AIO-SL.AAV8$^{\Delta VP2}$ Corrects Fah Deficiency *In Vivo*

Finally, the self-linearizing vector AIO-SL packaged into VP2-depleted AAV8 capsids was directly administered to adult Fah$^{-/-}$ animals (5×10^{10} vg per mouse) (Figure 5A).

Initially, the repair rate in a non-selective system was determined by injecting animals that were permanently kept on NTBC. Four weeks post-injection, single Fah-positive cells were observed in representative liver sections (Figure 5B). To further quantify genome editing efficiency, the loss of neoR was determined via qPCR and found to be 14.1% ± 5.96% (n = 5) (Figure 5C and Table 1). NGS analysis of the corresponding

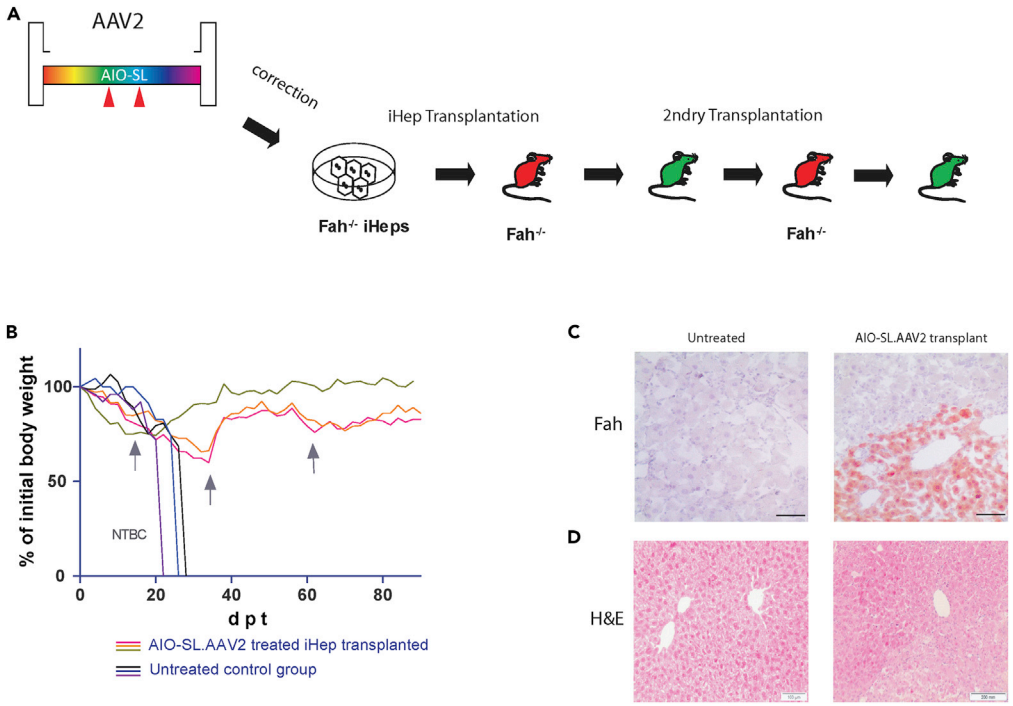

Figure 4. Gene Correction in *trans*-differentiated MEFs and Subsequent Transplantation Yields Phenotype Rescue

(A) Fah correction procedure and subsequent transplantation of Fah-corrected iHeps.

(B) Weight of Fah$^{-/-}$ mice transplanted (or not, n = 3) with AIO-SL.AAV2$^{\Delta VP2}$ Fah-corrected iHeps (dpt = days post-transplantation). Untreated mice that did not receive NTBC served as negative controls. NTBC was administered in short periods, when body weight dropped below 80% of initial weight.

(C) Immunohistochemical staining of FAH protein in representative liver paraffin sections of untreated or transplanted animals. Scale bar, 100 μm.

(D) H&E staining of liver sections of transplanted or non-transplanted animals. Scale bar, 200 μm.

fraction revealed donor integration rates from 10% up to 71% (Table 2), yielding a total knockin efficiency of 1.4%–9%.

To trigger the selection of Fah-corrected hepatocytes, NTBC was withdrawn on the day of injection in another cohort of animals and only provided intermittently, if required. Control animals showed a rapid deterioration of body weight and general health, whereas AIO-SL.AAV8$^{\Delta VP2}$-injected animals stabilized body weight within approximately 40 days and survived long-term without NTBC (Figure 5D). In liver tissue of these long-term surviving mice, Fah mRNA expression was detected via RT-qPCR (Figure 5E). Robust repopulation of Fah gene-corrected hepatocytes could be observed by staining of the FAH protein (Figures 5F and S3). To obtain a representative overview of the number of corrected genomes in a repopulated liver of an animal, DNA from the entire organ was collected and pooled, and editing efficiency with respect to neoR removal was measured by qPCR. In ~22% of the genomes, the neoR cassette was absent, indicating that the two DSBs had occurred (Figure 5G, blue/red pie chart). Further analysis of the corresponding PCR product via NGS revealed that 64.3% of those genomes lacking the neoR cassette had properly integrated the donor template (Figure 5G, green/orange pie chart and Table 3). Thus, the overall donor integration efficiency in the liver amounts to approximately 14%.

Analysis of Vector Genomes

As the all-in-one vector strategy demonstrated efficacy in particular *in vivo*, we finally investigated whether VP2 depletion indeed affects the AAV packaging capacity. To this end, the AIO-SL construct was packaged into AAV2 and AAV8 serotype capsids with and without VP2, respectively. Hence, we generated four conditions to be tested and further characterized: (i) AIO-SL_AAV8^{VP1-3} (ii) AIO-SL_AAV8$^{\Delta VP2}$ (iii) AIO-SL_AAV2^{VP1-3} and (iv) AIO-SL_AAV2 $^{\Delta VP2}$. To elucidate whether our construct can be packaged in its

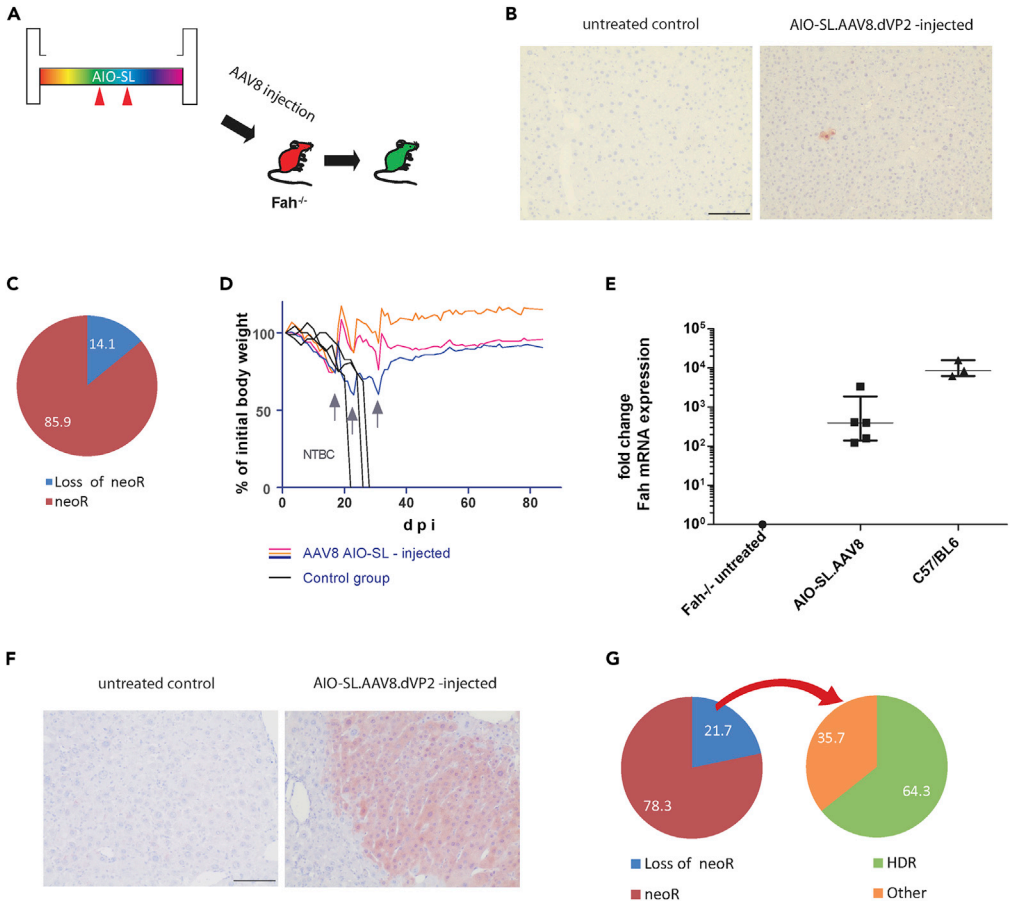

Figure 5. Single Administration of AIO-SL.AAV8$^{\Delta VP2}$ Mediates *In Vivo* Gene Correction

(A) Schematic illustration of direct administration of AIO.SL via AAV8 tail vein injection.

(B) Representative immunohistochemical staining for FAH protein in liver sections obtained from mice injected with AIO-SL.AAV8ΔVP2 and continuously kept on NTBC. Scale bar, 100 μm.

(C) Genome editing analysis of a representative sample from whole-liver genomic DNA using qPCR (n = 5). The blue/red pie chart represents the ratio of neoR removal caused by simultaneous DSBs. Individual values are listed in Table 2.

(D) Weight of animals injected with AIO-SL.AAV8$^{\Delta VP2}$ or not (n = 3, dpi = days post-injection). Same untreated controls as depicted in Figure 4B. NTBC administration, when required, is indicated by blue arrows.

(E) Detection of Fah mRNA by qRT-PCR in tissue derived from untreated mice (n = 1), AIO-SL.AAV8$^{\Delta VP2}$-injected mice (n = 3 biological replicates; in two of three animals, tissue samples are derived from two different liver lobes, therefore n = 5), and C57BL/6 wild-type mice (n = 3). Mean Ct values of untreated liver mRNA samples were set to 1, and differences were calculated using 2^{-ddCt} method.

(F) Representative immunohistochemical staining for FAH protein in liver sections obtained from mice with repopulated livers after AIO-SL.AAV8$^{\Delta VP2}$ injection and NTBC withdrawal. Scale bar, 100 μm.

(G) Genome editing analysis of a representative sample from whole-liver genomic DNA using qPCR (n = 5 technical replicates) and NGS. The blue/red pie chart represents the ratio of neoR removal obtained by simultaneous DSBs. Individual values are listed in Table 3. The green/orange pie chart displays the relative amount of HDR events (green area) after neoR removal.

entirety, viral DNA was isolated from iodixanol-purified AAVs and subjected to qPCRs using primer pairs targeting 3′-, central, and 5′-regions of the AAV genome (Figure 6A). Here, differences for 3′ and 5′ amplicons compared with the central amplicon were detected and are shown as percentage of the central amplicon number (Figure 6A). However, as depicted in Figure 6B, the qPCR method does not allow to distinguish whether one molecule is truncated 5′ and 3′ (i), 5′ or 3′ (ii, iii), or not at all (iv). To analyze the qPCR "blind" range below the red dashed line exemplarily shown in Figure 6A (iv), Southern blot (Sambrook and Russell, 2006) analysis was performed (Figure 6C). DNA obtained from all four viral vector preparations exhibits a distinct pattern of bands, namely, ~6 kb, ~5 kb, ~4 kb, and lower. The full-length band in

	(%) HDR	(%) Other		(%) HDR	(%) Other
AIO-NL_1	12.5	87.5	AIO-SL_1	54.9	45.1
AIO-NL_2	7.6	92.4	AIO-SL_2	51.9	48.1
AIO-NL_3	7.2	92.8	AIO-SL_3	66.8	33.2
AIO-NL_4	9.3	90.7	AIO-SL_4	60.6	39.4
AIO-NL Mean	9.15	90.85	AIO-SL Mean	58.55	41.45

Table 1. Analysis of Donor Integration Events Determined via NGS in Cell Culture
Genomic DNA of transduced MEFs was isolated and employed for NGS analysis as described in Figure S1.

Figure 6C, lane 2, appears rather weak, whereas a different viral vector preparation of AIO-SL.AAV8$^{\Delta VP2}$ previously used for *in vivo* experiments, exhibits much higher intensity of this band (Figure 6C, lanes 2a and 2b). This striking difference in full-length to truncated genome ratio, however, does not become apparent in the corresponding qPCR analysis of this production (Figure S4A), which underlines the advantage of Southern blot analysis.

As the above-mentioned truncation analysis does not provide information about the functionality of the viral vector particles, AAV genome integrity upon *in vivo* application was investigated. To this end, both AAV8 vector preparations depicted in Figure 6C (lanes 1 and 2) were injected into Fah$^{-/-}$ mice and liver DNA was analyzed via qPCR after 4 weeks (Figures S4B and S4C). Comparison of the integrity of viral vector DNA after production and from vector-treated hepatocytes revealed essential variation (Figures 6A, S4B, and S4C).

Interestingly, the ~6-kb band representing full-length genomes was only detectable in the AAV8 serotype, but not in AAV2 (Figure 6C, lanes 1 and 2). To obtain a better overview of the distribution of vector genomes, the four variants were again produced and purified using continuous cesium chloride density gradient purification, which enables a better resolution of particle populations than iodixanol purification (Strobel et al., 2015). Southern blot analysis of various fractions ranging from refractive index 1.37 to 1.35 suggests a superior packaging capacity for the AAV8 serotype, independent of VP2 abundance (Figure S5).

To test whether this phenomenon also applies for other oversized recombinant vector genomes, we packaged four different constructs of gradually increasing genome size (5.15, 5.5, 5.8, and 6.17 kb) into AAV2 and AAV8 particles (Figure 6D) (Fakhiri et al., 2019). These constructs harbor a different transgene (SpCas9) driven by a different promoter. Viral vector DNA of the preparations was isolated and equal volumes were analyzed by Southern blotting (Figure 6E). The resulting bands suggest a maximum cargo size of approximately 5.2 kb for AAV2, whereas AAV8 appears to package vector genomes clearly exceeding this threshold.

DISCUSSION

Successful *ex vivo* gene editing has been demonstrated in hematopoietic stem cells, which corrected blood-borne hereditary abnormalities upon cell transplantation in mice (Dever et al., 2016). In contrast,

	% Loss of neoR	% neoR	NGS (% Other)	NGS (% HDR)
AIO-SL + NTBC_1	22.08	77.91	89.5	10.5
AIO-SL + NTBC_2	9.98	90.02	NA	NA
AIO-SL + NTBC_3	8.94	91.06	NA	NA
AIO-SL + NTBC_4	8.72	91.27	26.7	73.3
AIO-SL + NTBC_5	20.54	79.46	28.9	71.1

Table 2. Quantification of Initial Editing Efficiency *In Vivo*
Genomic DNA obtained from Fah$^{-/-}$ mice injected with AIO-AAV8^{dVP2} and continuously kept on NTBC was analyzed via qPCR and NGS as described above.

	% Loss of neoR	% neoR	NGS (% Other)	NGS (% HDR)
AIO-SL_left lobe 1	38.73	61.27		
AIO-SL_left lobe 2	19.4	80.6		
AIO-SL_right lobe	15.5	84.5		
AIO-SL_median lobe	16.5	83.5		
AIO-SL_caudate lobe	18.6	81.4		
Pooled			35.7	64.3

Table 3. Quantification of Editing Efficiency upon NTBC Withdrawal

Genomic DNA of a repopulated animal was isolated lobe-wise and analyzed via neoR qPCR. A Fah-specific PCR product derived from a pool of samples was analyzed via NGS.

for correction of hereditary diseases in solid large organs such as the liver, substantial technical hurdles remain, such as the size of transgenes that can be packaged into AAV, which has a natural genome size of ~4.7 kb.

In our single-vector approach, we combined all components necessary for gene excision and replacement on one single molecule. Despite optimal design (220-bp arms of homology), the vector genome has a size of 5.73 kb (without ITRs), which still substantially exceeds the optimal size of 4.675 kb (which includes ITRs). Based on results of various studies (Grieger and Samulski, 2005) (Wu et al., 2010) (Dong et al., 2010) (Hirsch et al., 2016), vector genomes of 4.9 kb are tolerated without affecting packaging efficiency or infectivity. Furthermore, intact vector genomes rather than 5′ truncated versions are delivered. In particular with regard to the latter issue, the threshold seems to be reached at 5 kb (Wu et al., 2010). According to the qPCR and Southern blot analysis of four distinct vectors (AAV2 and AAV8 with or without VP2-deletion), we detected 5′ and 3′ truncations with all designs, which is in line with the above-mentioned studies.

Intriguingly, however, in the case of our AIO-SL construct, the packaging capacity of AAV8 appears to be superior over AAV2 as demonstrated in Figures 6C and S5A–S5D. This fact might explain the difference in efficiency when comparing our results obtained *ex vivo* with those obtained *in vivo*. Specifically, we employed AIO-SL.AAV2$^{\Delta VP2}$ for genome editing *in vitro*, which according to our results most likely relied on intracellular recombination events producing complete genomes. In contrast, less AIO-SL.AAV8$^{\Delta VP2}$ was needed *in vivo*, perhaps due to the higher level of full-length genomes that was transferred. Thus, the AAV8 capsid with or without VP2 seems more suitable for the delivery of our oversized AIO-SL vector genome.

Regarding the packaging of our oversized vector, Southern blot analysis did not indicate any advantage, or disadvantage, of the VP2 mutant in the ~6-kb range for AAV2 and AAV8. Our results are thus in line with the findings of Grieger and Samulski, who have examined this strategy for AAV serotypes 1–5 (Grieger and Samulski, 2005).

The observation of enhanced cargo capacity of AAV8 was further supported by exploring vector genomes of increasing length encoding for a different transgene (SpCas9). Also here, we noticed evident differences within the 5- to 6-kb range when comparing both serotypes (Figure 6E). Successful AAV8 vector-mediated delivery of the 5.6-kb canine FVIII transgene (Sarkar et al., 2003) substantiates our findings. However, further investigations are required to elucidate whether this phenomenon holds true for other (therapeutic) oversized genes such as base editors (Gaudelli et al., 2017). Therefore, concerning the packaging of oversized recombinant AAV genomes, the choice of AAV serotype appears to be of importance.

Additional bands suggest incomplete vector genomes below the natural packaging limit. This effect may have been caused by a putative artificial packaging signal of the SaCas9 gRNA scaffold (Xie et al., 2017). As the ubiquitous ~4-kb band subtly matches with the size of a fragment from 3′ ITR to one of the SaCas9 gRNA scaffold, we analyzed the potential DNA secondary structure of this scaffold using mfold (Figure S6) (Zuker, 2003). Intriguingly, the SaCas9 gRNA scaffold sequence exhibits an ITR-like DNA structure, which

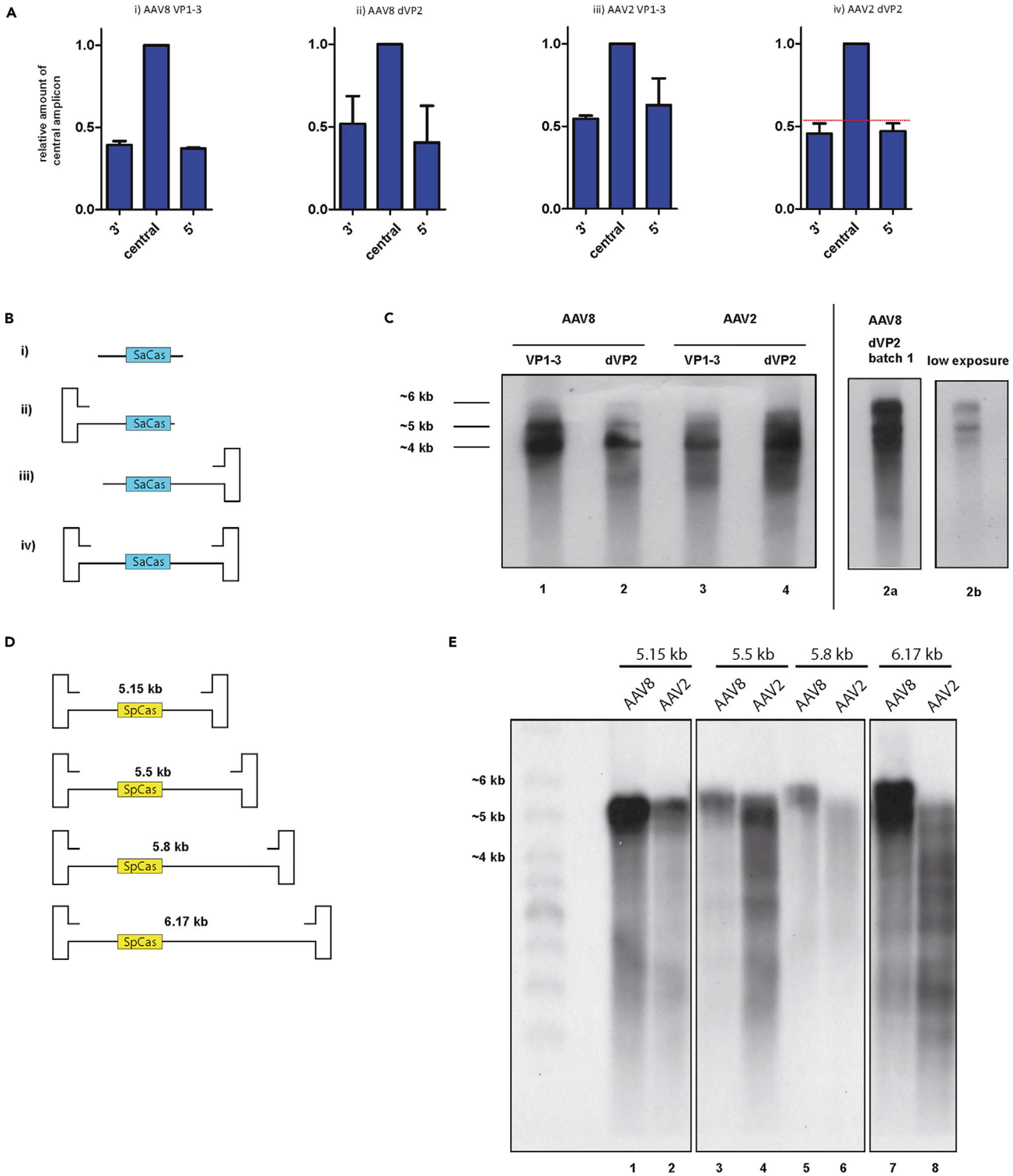

Figure 6. Analysis of Viral Vector Genomes

(A) qPCR analysis of vector integrity using three amplicons depicted in Figure 2A (green lines). Viral DNA of different AAV preparations was isolated and employed for qPCR. Number of preparations: AIO-SL.AAV8^{VP1-3} (n = 1), AIO-SL.AAV8$^{\Delta VP2}$ (n = 3), AIO-SL.AAV2^{VP1-3} (n = 2), and AIO-SL.AAV2$^{\Delta VP2}$ (n = 3). The number of detected 3′ and 5′ amplicons is depicted relative to the central amplicon number. The red dashed line shown in (iv) symbolizes the qPCR-blind range to be further analyzed via Southern blotting.

Figure 6. *Continued*

(B) Depiction of AAV genome truncation scenarios not to be distinguished via qPCR: (i) full-length versus (ii) 5′ truncation and (iii) 3′ truncation.

(C) Autoradiograph of Southern blot. Detection of recombinant AAV genomes using a SaCas9-specific radiolabeled probe. Full-size recombinant AAV genomes can be detected at ~6 kb. Truncated versions are detectable at ~5 kb, ~4 kb, and lower. Lanes 2a and 2b represent viral DNA isolated from a different production of AIO-SL.AAV8$^{\Delta VP2}$.

(D) Depiction of four recombinant AAV vectors of gradually increasing genome size.

(E) Southern blot of viral vector DNA obtained from iodixanol-purified AAV2 and AAV8 preparations based on the vectors depicted in (D). Here, a SpCas9-specific radiolabeled probe was employed for detection.

may exist *in vivo* and serve as a packaging signal. Additional experiments will be required to test whether the SaCas9 gRNA scaffold sequence contains a functional packaging signal.

Initially, upon induction of two simultaneous DSBs without providing a donor template, we observed that indel-free repair appeared to be the preferred repair pathway, as the majority of DNA fragment deletions aligned perfectly. This interesting phenomenon may already be therapeutically useful and could be employed for precise excision of pathology-associated genomic regions, such as trinucleotide repeats predominantly present in various neurodegenerative diseases (MacDonald et al., 1993).

Earlier published findings substantiate our observation regarding the self-linearizing repair template (Zhang et al., 2017) (Suzuki et al., 2016). An "all-in-one" vector lacking the ability to self-linearize did not achieve comparable levels of donor integration (Figure 3C). Consequently, the critical modification responsible for the enhancement of donor integration appears to be self-linearization, perhaps due to better accessibility to the DNA repair machinery.

Our *in vitro*-generated iHeps remain as immature hepatocytes, as they cannot fully mimic functions of primary hepatocytes as analyzed previously (Song et al., 2016). However, our *ex vivo*-corrected iHeps rescue Fah$^{-/-}$ mice completely as the animals survived more than half a year without NTBC, suggesting that an *in vivo* niche may further enhance the functional maturation of iHeps. Corrected iHeps may thus become a suitable therapeutic option.

Notably, a single injection of AIO-SL.AAV8Δ^{VP2} corrected the disrupted Fah gene and resulted in robust repopulation of the liver by FAH-positive hepatocytes. The qPCR and NGS analyses of liver DNA of repopulated animals indicate that roughly 14% of the genomes were corrected via donor integration, which may appear rather low. It has been shown that the grade of polyploidy in the liver increases with age, thereby leading to the formation of hepatocytes with additional sets of chromosomes (e.g., $\geq$8n) (Duncan et al., 2010). Therefore, a repair rate of ~14% of the liver genomes may not necessarily correspond to only 14% of the hepatocytes because a cell with one single Fah-corrected allele could produce sufficient amounts of FAH. In addition, the liver consists of approximately 40% non-hepatocyte cell types that are, if at all, inefficiently transduced by AAV8 (Rezvani et al., 2016). As these cells were also incorporated into the whole-liver DNA analysis, the number of positive sequencing results indicating donor integration likely underestimates that actual efficiency. Conclusively, we demonstrate successful *ex vivo* and *in vivo* gene editing after delivery of an all-in-one vector by AAV particles. Our approach of large fragment excision combined with donor template integration mediated by a single vector could be promisingly optimized by utilizing the recently published Cas9 variant CasX (Liu et al., 2019).

Limitations of the Study

During this study, we have encountered clear differences in packaging limitation of oversized vector genomes in AAV2 and AAV8. Indeed, we have successfully re-evaluated this observation using constructs different from our vector, but still, further characterization (e.g., infectivity, stability) of viral vector particles harboring oversized genomes may be required.

As AAV8 turned out to be more suitable for the delivery of our AIO-SL construct, it could have been consistently used throughout the study, even though it presents low transduction efficiencies in cultured cells.

METHODS

All methods can be found in the accompanying Transparent Methods supplemental file.

SUPPLEMENTAL INFORMATION

Supplemental Information can be found online at https://doi.org/10.1016/j.isci.2019.100764.

ACKNOWLEDGMENTS

The study was supported by grants from the Deutsche Forschungsgemeinschaft (DFG: OT131/6-1, EXC 62/2 to M.O., SH640/1-2, 188/9-1, SFB-738 to A.D.S., and EXC81, SFB1129-TP2/16 and TRR179-TP18 to D.G., Projektnummern 240245660 and 272983813), a stipend to S.K. from the Studienstiftung des Deutschen Volkes, a grant from the Cystic Fibrosis Foundation (CFF, grant number GRIMM15XX0) to J.F. and D.G., and the Bundesministerium für Bildung und Forschung (BMBF) and MWK Lower Saxony-funded Professorinnenprogramm Niedersachsen to H.B. We thank Stefanie Stahnke for cloning the pRC-VP2k.o. and pXR8VP2k.o. plasmids, Jasper Götting for assistance during library preparation, and Elke Barczak and Nicki Lenort for viral vector production and qPCR analysis.

AUTHOR CONTRIBUTIONS

M.O., H.B., S.K., and A.D.S. conceived the idea, S.K., M.O., H.B., F.S., J.B., A.S., and A.D.S. designed the experiments. S.K., Z.D, Q.Y., and A.R. performed the experiments with significant support from A.D., A.B., L.S., S.S., T.Y., and J.F. M.O., H.B., and S.K. wrote the manuscript with important contributions from D.G., F.S., and J.B.

DECLARATION OF INTERESTS

The authors declare no competing interests.

Received: October 8, 2018
Revised: October 2, 2019
Accepted: December 9, 2019
Published: January 24, 2020

REFERENCES

Bassing, C.H., and Alt, F.W. (2004). The cellular response to general and programmed DNA double strand breaks. DNA Repair *3*, 781–796.

Bleker, S., Pawlita, M., and Kleinschmidt, J.A. (2006). Impact of capsid conformation and Rep-capsid interactions on adeno-associated virus type 2 genome packaging. J. Virol. *80*, 810–820.

Cristea, S., Freyvert, Y., Santiago, Y., Holmes, M.C., Urnov, F.D., Gregory, P.D., and Cost, G.J. (2013). In vivo cleavage of transgene donors promotes nuclease-mediated targeted integration. Biotechnol. Bioeng. *110*, 871–880.

Dever, D.P., Bak, R.O., Reinisch, A., Camarena, J., Washington, G., Nicolas, C.E., Pavel-Dinu, M., Saxena, N., Wilkens, A.B., Mantri, S., et al. (2016). CRISPR/Cas9 β-globin gene targeting in human haematopoietic stem cells. Nature *539*, 384–389.

Dong, B., Nakai, H., and Xiao, W. (2010). Characterization of genome integrity for oversized recombinant AAV vector. Mol. Ther. *18*, 87–92.

Duncan, A.W., Taylor, M.H., Hickey, R.D., Hanlon Newell, A.E., Lenzi, M.L., Olson, S.B., Finegold, M.J., and Grompe, M. (2010). The ploidy conveyor of mature hepatocytes as a source of genetic variation. Nature *467*, 707–710.

Ellis, B.L., Hirsch, M.L., Barker, J.C., Connelly, J.P., Steininger, R.J., 3rd, and Porteus, M.H. (2013). A survey of ex vivo/in vitro transduction efficiency of mammalian primary cells and cell lines with Nine natural adeno-associated virus (AAV1-9) and one engineered adeno-associated virus serotype. Virol. J. *10*, 74.

Fakhiri, J., Schneider, M.A., Puschhof, J., Stanifer, M., Schildgen, V., Holderbach, S., Voss, Y., El Andari, J., Schildgen, O., Boulant, S., et al. (2019). Novel Chimeric gene therapy vectors based on adeno-associated virus and four different mammalian Bocaviruses. Mol. Ther. Methods Clin. Dev. *12*, 202–222.

Gaudelli, N.M., Komor, A.C., Rees, H.A., Packer, M.S., Badran, A.H., Bryson, D.I., and Liu, D.R. (2017). Programmable base editing of A•T to G•C in genomic DNA without DNA cleavage. Nature *551*, 464–471.

Grieger, J.C., and Samulski, R.J. (2005). Packaging capacity of adeno-associated virus serotypes: impact of larger genomes on infectivity and postentry steps. J. Virol. *79*, 9933–9944.

Grompe, M., al-Dhalimy, M., Finegold, M., Ou, C.N., Burlingame, T., Kennaway, N.G., and Soriano, P. (1993). Loss of fumarylacetoacetate hydrolase is responsible for the neonatal hepatic dysfunction phenotype of lethal albino mice. Genes Dev *7*, 2298–2307.

Hirsch, M.L., Wolf, S.J., and Samulski, R.J. (2016). Delivering transgenic DNA exceeding the Carrying capacity of AAV vectors. Methods Mol. Biol. 21–39, https://doi.org/10.1007/978-1-4939-3271-9_2.

Jinek, M., East, A., Cheng, A., Lin, S., Ma, E., and Doudna, J. (2013). RNA-programmed genome editing in human cells. Elife *2*, e00471.

Junge, N., Yuan, Q., Vu, T.H., Krooss, S., Bednarski, C., Balakrishnan, A., Cathomen, T., Manns, M.P., Baumann, U., Sharma, A.D., and Ott, M. (2018). Homologous recombination mediates stable Fah gene integration and phenotypic correction in tyrosinaemia mouse-model. World J. Hepatol. *10*, 277–286.

Liu, J.J., Orlova, N., Oakes, B.L., Ma, E., Spinner, H.B., Baney, K.L.M., Chuck, J., Tan, D., Knott, G.J., Harrington, L.B., et al. (2019). CasX enzymes comprise a distinct family of RNA-guided genome editors. Nature *566*, 218–223.

MacDonald, M.E., Ambrose, C.M., Duyao, M.P., Myers, R.H., Lin, C., Srinidhi, L., Barnes, G., Taylor, S.A., James, M., Groot, N., MacFarlane, H., et al. (1993). A novel gene containing a trinucleotide repeat that is expanded and unstable on Huntington's disease chromosomes. The Huntington's Disease Collaborative Research Group. Cell *72*, 971–983.

Nakai, H., Fuess, S., Storm, T.A., Muramatsu, S., Nara, Y., and Kay, M.A. (2005). Unrestricted hepatocyte transduction with adeno-associated virus serotype 8 vectors in mice. J. Virol. *79*, 214–224.

Nathwani, A.C., Reiss, U.M., Tuddenham, E.G., Rosales, C., Chowdary, P., McIntosh, J., Della Peruta, M., Lheriteau, E., Patel, N., Raj, D., et al. (2014). Long-term safety and efficacy of factor IX

gene therapy in hemophilia B. N Engl J Med *371*, 1994–2004.

Paulk, N.K., Wursthorn, K., Wang, Z., Finegold, M.J., Kay, M.A., and Grompe, M. (2010). Adeno-associated virus gene repair corrects a mouse model of hereditary tyrosinemia in vivo. Hepatology *51*, 1200–1208.

Pinello, L., Canver, M.C., Hoban, M.D., Orkin, S.H., Kohn, D.B., Bauer, D.E., and Yuan, G.C. (2016). Analyzing CRISPR genome-editing experiments with CRISPResso. Nat. Biotechnol. *34*, 695–697.

Rezvani, M., Español-Suñer, R., Malato, Y., Dumont, L., Grimm, A.A., Kienle, E., Bindman, J.G., Wiedtke, E., Hsu, B.Y., Naqvi, S.J., et al. (2016). In vivo hepatic reprogramming of myofibroblasts with AAV vectors as a therapeutic strategy for liver Fibrosis. Cell Stem Cell *18*, 809–816.

Sambrook, J., and Russell, D.W. (2006). Southern blotting: capillary transfer of DNA to membranes. CSH Protoc. *2006*, https://doi.org/10.1101/pdb.prot4040.

Sarkar, R., Tetreault, R., Gao, G., Wang, L., Bell, P., Chandler, R., Wilson, J.M., and Kazazian, H.H., Jr. (2003). Total correction of hemophilia A mice with canine FVIII using an AAV 8 serotype. Blood *103*, 1253–1260.

Smith, A., Collaco, R., and Trempe, J.P. (2004). AAV vector delivery to cells in culture. Methods Mol. Biol. *246*, 167–177. http://www.ncbi.nlm.nih.gov/pubmed/14970591, Accessed June 22, 2019.

Song, G., Pacher, M., Balakrishnan, A., Yuan, Q., Tsay, H.C., Yang, D., Reetz, J., Brandes, S., Dai, Z., Pützer, B.M., et al. (2016). Direct reprogramming of hepatic myofibroblasts into hepatocytes in vivo attenuates liver Fibrosis. Cell Stem Cell *18*, 797–808.

Strobel, B., Miller, F.D., Rist, W., and Lamla, T. (2015). Comparative analysis of cesium chloride- and iodixanol-based purification of recombinant adeno-associated viral vectors for preclinical applications. Hum. Gene Ther. Methods *26*, 147–157.

Suzuki, K., Tsunekawa, Y., Hernandez-Benitez, R., Wu, J., Zhu, J., Kim, E.J., Hatanaka, F., Yamamoto, M., Araoka, T., Li, Z., et al. (2016). In vivo genome editing via CRISPR/Cas9 mediated homology-independent targeted integration. Nature *540*, 144–149.

Truong, D.J., Kühner, K., Kühn, R., Werfel, S., Engelhardt, S., Wurst, W., and Ortiz, O. (2015). Development of an intein-mediated split–Cas9 system for gene therapy. Nucleic Acids Res. *43*, 6450.

Warrington, K.H., Jr., Gorbatyuk, O.S., Harrison, J.K., Opie, S.R., Zolotukhin, S., and Muzyczka, N. (2004). Adeno-associated virus type 2 VP2 capsid protein is nonessential and can tolerate large peptide insertions at its N terminus. J. Virol. *78*, 6595–6609.

Wu, Z., Yang, H., and Colosi, P. (2010). Effect of genome size on AAV vector packaging. Mol. Ther. *18*, 80–86.

Xie, J., Mao, Q., Tai, P.W.L., He, R., Ai, J., Su, Q., Zhu, Y., Ma, H., Li, J., Gong, S., et al. (2017). Short DNA hairpins Compromise recombinant adeno-associated virus genome homogeneity. Mol. Ther. *25*, 1363–1374.

Xu, Z., Yue, Y., Lai, Y., Ye, C., Qiu, J., Pintel, D.J., and Duan, D. (2004). Trans-splicing adeno-associated viral vector-mediated gene therapy is limited by the accumulation of spliced mRNA but not by dual vector coinfection efficiency. Hum. Gene Ther. *15*, 896–905.

Yang, Y., Wang, L., Bell, P., McMenamin, D., He, Z., White, J., Yu, H., Xu, C., Morizono, H., Musunuru, K., et al. (2016). A dual AAV system enables the Cas9-mediated correction of a metabolic liver disease in newborn mice. Nat. Biotechnol. *34*, 334–338.

Yin, H., Xue, W., Chen, S., Bogorad, R.L., Benedetti, E., Grompe, M., Koteliansky, V., Sharp, P.A., Jacks, T., and Anderson, D.G. (2014). Genome editing with Cas9 in adult mice corrects a disease mutation and phenotype. Nat. Biotechnol. *32*, 551–553.

Yin, H., Song, C.Q., Dorkin, J.R., Zhu, L.J., Li, Y., Wu, Q., Park, A., Yang, J., Suresh, S., Bizhanova, A., et al. (2016). Therapeutic genome editing by combined viral and non-viral delivery of CRISPR system components in vivo. Nat. Biotechnol. *34*, 328–333.

Zhang, J.P., Li, X.L., Li, G.H., Chen, W., Arakaki, C., Botimer, G.D., Baylink, D., Zhang, L., Wen, W., Fu, Y.W., et al. (2017). Efficient precise knockin with a double cut HDR donor after CRISPR/Cas9-mediated double-stranded DNA cleavage. Genome Biol. *18*, 35.

Zuker, M. (2003). Mfold web server for nucleic acid folding and hybridization prediction. Nucleic Acids Res. *31*, 3406–3415.

iScience, Volume *23*

Supplemental Information

Ex Vivo/*In vivo* Gene Editing in Hepatocytes Using "All-in-One" CRISPR-Adeno-Associated Virus Vectors with a Self-Linearizing Repair Template

Simon Alexander Krooss, Zhen Dai, Florian Schmidt, Alice Rovai, Julia Fakhiri, Akshay Dhingra, Qinggong Yuan, Taihua Yang, Asha Balakrishnan, Lars Steinbrück, Sangar Srivaratharajan, Michael Peter Manns, Axel Schambach, Dirk Grimm, Jens Bohne, Amar Deep Sharma, Hildegard Büning, and Michael Ott

Supplemental Information

Supplemental Figure 1

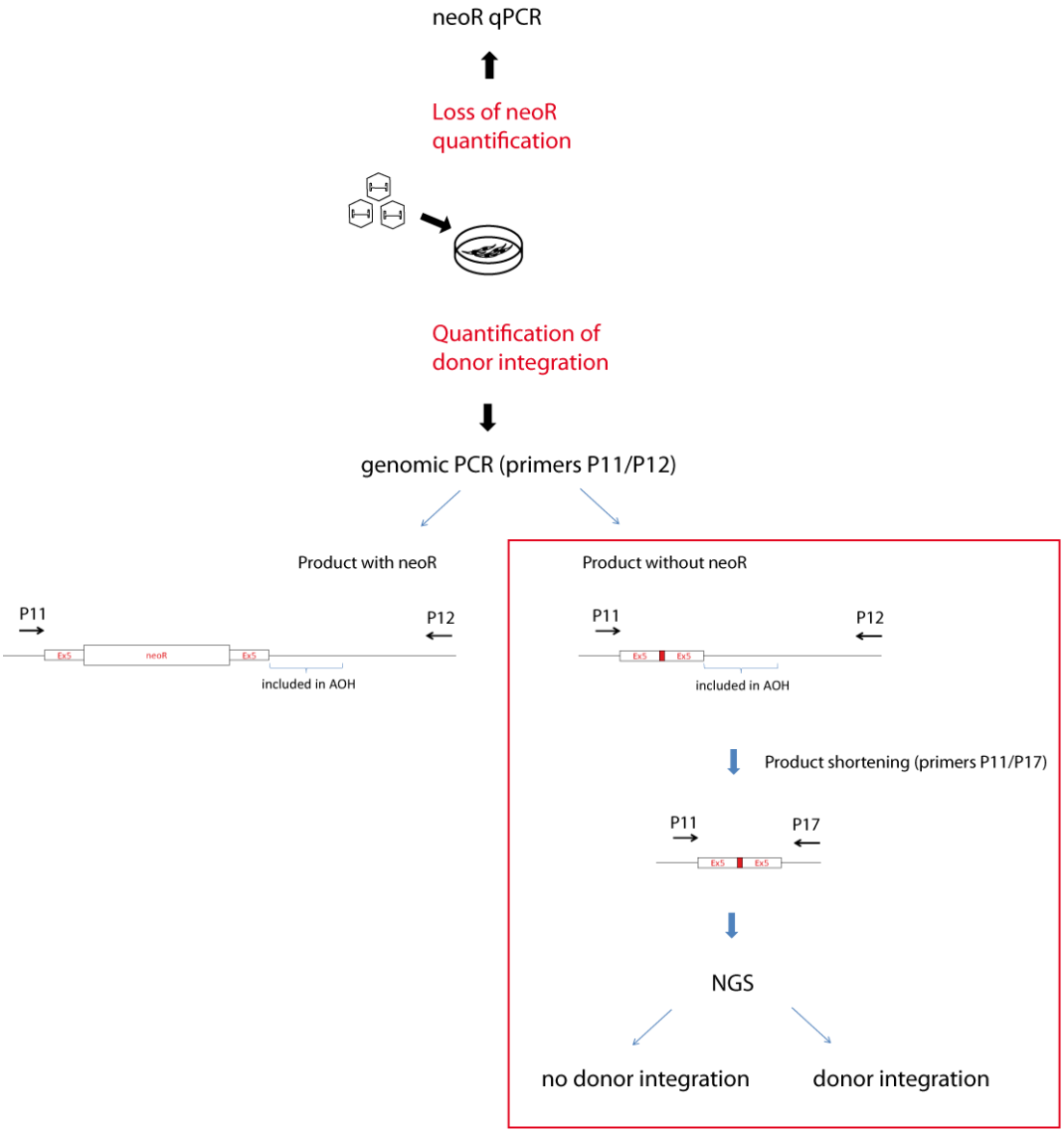

Figure S1 | Schematic overview of workflow to determine editing efficiency related to Figure 3c. Genomic DNA of cells was collected 14 days post AAV transduction. To identify the number of genomes without neoR, a qPCR targeting the neoR sequence was performed. Loss of neomycin is calculated by 100 – value of neoR qPCR. Donor integration rate was determined by analysis of a PCR product generated by P11/12 to exclude Fah Exon 5 amplicons derived from viral vector genomes. NGS was performed on the above mentioned PCR product shortened by P11/P17.

Supplemental Figure 2

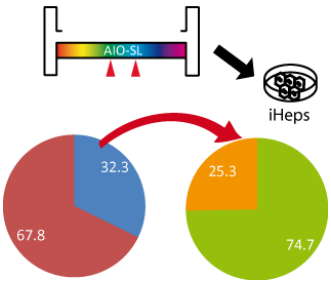

Figure S2 | Evaluation of editing efficiency in iHeps related to Figure 3.

qPCR based quantification of neoR removal in AIO-SL.AAV2$^{\Delta VP2}$-treated iHeps (n=3, SD= 2.4). The blue/red pie chart depicts the loss of neoR ratio as determined via qPCR (loss of neomycin = 100 - neoR). The green/orange pie chart depicts the percentage of donor integration reads (green) versus other repair (orange) determined via NGS and refers to the number of reads lacking neoR (blue area). Genomic DNA of treated cells was subjected to PCR strategies depicted in Figure S1.

Supplemental Figure 3

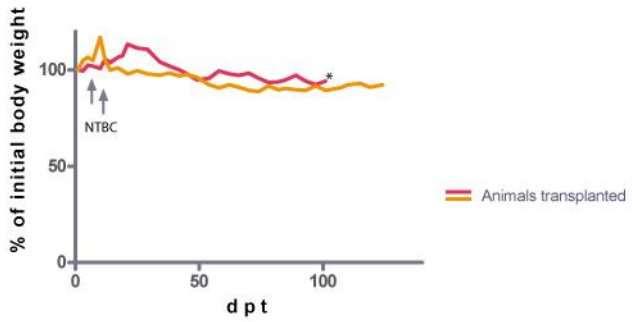

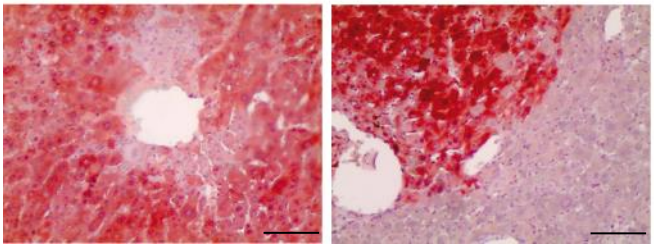

Figure S3 | Long term survival after secondary transplantation and liver repopulation upon in vivo Fah correction related to Figure 4. Hepatocytes from mice that were initially

transplanted AIO-SL.AAV2 $^{\Delta VP2}$-treated iHeps were isolated after 3 months and 1×10^6 cells were injected into the spleen of recipient mice (d p t = days post transplantation).

Staining: Mice injected with AIO-SL.AAV8 $^{\Delta VP2}$ were set off NTBC. Three months post injection, liver samples were collected and stained for FAH protein. Scale bar = 100 µm.

Supplemental Figure 4

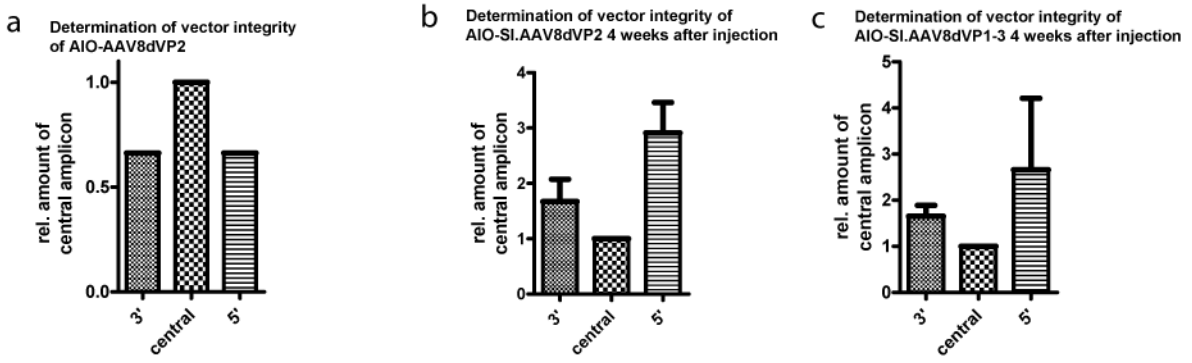

Figure S4 | qPCR analysis of vector integrity using three amplicons depicted in figure 2a), related to Figure 6.

a) Viral vector DNA of an AIO-SL.AAV8$^{\Delta VP2}$ (batch 1) production was employed for qPCR using primer pairs P24-P29. Amount of 3' and 5' amplicons is depicted as a fraction of the central amplicon. **b)** qPCR detecting truncations was performed on liver genomic DNA obtained from animals injected with AIO-SL_AAV8$^{\Delta VP2}$ and sacrificed four weeks upon injection. Animals were permanently kept on NTBC (n=4, SD 3': 0.348, SD 5': 0.475). **c)** Analysis of vector integrity as described in b) was performed from genomic DNA of animals injected with AIO-SL_AAV8^{VP1-3}.

Supplemental Figure 5

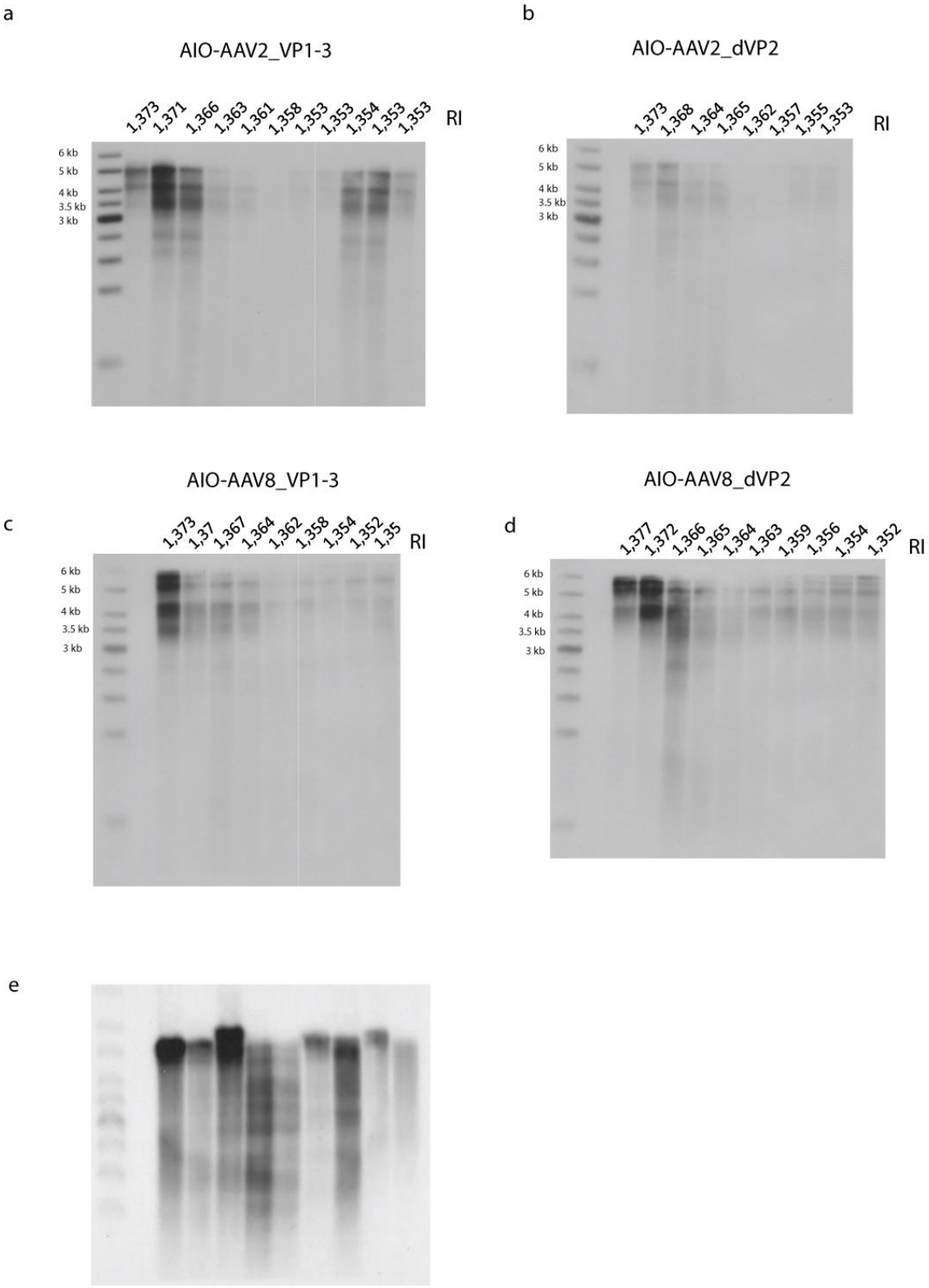

Figure S5 | Autoradiographs of Southern Blots detecting AAV genomes related to Figure 6. Detection of recombinant AAV genomes was achieved using a SaCas9 specific radiolabeled

probe. Viral vector DNA of **a)** AIO-SL_AAV8VP1-3, **b)** AIO-SL_AAV8dVP2, **c)** AIO-SL_AAV2VP1-3, and **d)** AIO-SL_AAV2dVP2 was isolated upon cesium chloride purification. Various fractions of different refractive indices (RI) were loaded and separated under denaturing conditions. Full length recombinant AAV genomes can be detected at ~6kb. Truncated versions are detectable at ~5kb, ~4kb and lower. **e)** Unprocessed Southern blot from **Figure 6e**.

Supplemental Figure 6

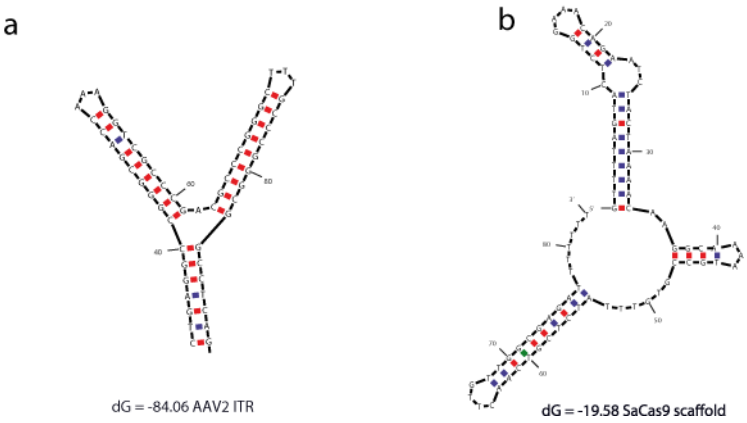

Figure S6 | **Prediction of DNA secondary structures related to Figure 6.** Sequences of AAV2 ITR and SaCas9 scaffold were analyzed using DNA folding algorithm mfold(Zuker 2003).

Supplemental Tables

Table S1 | **Oligonucleotides used for PCR and qPCR analysis as well as for cloning works related to Figure 1, 2, 5 and 6.**

P1:	Donor-aio-for	5’-ggccgcgctcAGTTGTTGACCTCGACTGCCGAGgagggtactggcagctactt-3’
P2:	Donor-aio-rev	5’-agggcgcgccTGGTGGTCGAGGCTAGAACTActggatagcctaggacctc-3’
P3:	U6-aio-for	5’-cgg cgg ccg ccg agt cca aca ccc g-3’
P4:	U6-aio-rev	5’-cagtaccctcCTCGGCAGTCGAGGTCAACAACTgagcgcggccacaaaaaaatc-3’
P5:	7SK-aio-for	5’-ggctatccagTAGTTCTAGCCTCGACCACCAggcgcgccctgcagtattt-3’
P6:	7SK-aio-rev	5’-ccgcggtaccgcaaaaaaatctcgc-3’
P7:	Neo2qPCR for	5’-CGACCACCAAGCGAAAC T-3’
P8:	Neo2qPCR rev	5’-CGACAAGACCGGCTTCCAT-3’
P9:	GAPDH qPCR for	5’-TTCACCACCATGGAGAAGGC-3’
P10:	GAPDH qPCR rev	5’-GGCATGGACTGTGGTCATGA-3’
P11:	Ex5 for	5’-CTGTTTGGGGTGTTCCCTCT-3’
P12:	700rev	5’-CgTCTAgATCAggCTgTgTTTATCCCCAg-3’
P13:	700for	5’-gCgAATTCTgACAATTgAgCAAAAgTCTg-3’
P14:	1,4neo for	5’-GTCCAGATCATCCTGATCGACA-3’
P15:	1,4ne rev	5’-TGCATACGCTTGATCCGGCTAC-3’
P16:	Ex5 rev	5’-CCAGCATCTGGTCTAGGACATAC-3’
P17	200 rev	5’-CgTCTAgAgATAggCTggATAgCCTAggA-3’
P18	Fah Ex5 qPCR for	5’-AGAATGCGCTGTTGCCAAA-3’
P19	Fah Ex5 qPCR rev	5’-GGAAGCTCGGCCATGGTAT-3’
P20	sgRNA5’_fw	5’-CACCGTTGTTGACCTCGACTGCCGAG-3’

P21	sgRNA5'_rv	5'-AAACCTCGGCAGTCGAGGTCAACAAC-3'
P22	sgRNA3' _fw	5'-CACCGTTGGTGGTCGAGGCTAGAACTA-3'
P23	sgRNA3'_rv	5'-AAACTAGTTCTAGCCTCGACCACCAAC-3'
P24	qPCR LP1fw	5'-GTTTGCTCCTCCGATAACTG -3'
P25	qPCR LP1rv	5'-ACCTTAGAGTCCGGATTCAC -3'
P26	qPCR SaCasfw	5'- GAACAACCTGGACGTGAAAG-3'
P27	qPCR SaCasrv	5'- GAAGATGAAATCGGCGTTGG-3'
P28	qPCR U6fw	5'-GGAAATAGGCCCTCTTCCTG-3'
P29	qPCR U6rv	5'-GACACTGCTCGGTAGTTTCG-3'
P30	U6-aio-NL-REV	5'cagtacctcgagcgcggccacaaaaatc-3'
P31	7SK-aioNL-FOR	5'-GGCTATCCAGGGCGCGCCCTGCAGTATTT-3'
P32	NL-Donor-for	5'- ggccgcgctcgagggtactggcagctactt-3'
P33	NL-Donor-rev	5' agggcgcgccctggatagcctaggacctc-3'

Table S2 | Sequences of the synthesized donor template related to Figure 1 and reference sequence for NGS analyses related to Figure 3 and 5.

gBlock® sequence of the donor template

5'TCAGTCTGCGTTGTCCTGCAAGTCTGACACTATTGTCCATTTTTCTGGCCATCTATGATAAGTGGTACAAAAT
GAGAGGAGGGTACTGGCAGCTACTTCATATTTAAATCTCACTGTCTGATTCAGAAACTATGAACTTACTTTTTTT
TCCTGTGTTAAGGGGTCCTTGAATCTTGAAGAATGGTTTGAGCCCCTGCTTTTGGACCCGGGGTTCCTCCATCT
AGGTCAATGGCTGTTTGGGGTGTTCCCTCTGCAGGAGACTACACGGACTTCTACAGCTCTCGGCAGCATGCCA
CCAATGTTGGCATTATGTTCAGAGGCAAGGAGAATGCGCTGTTGCCAAATTGGTATGTCCTAGACCAGATGCT
GGGATAAATTCAAAGTCGGCTCTTCTCTACAGTATGTTTTTCCCAGCAGCAAAGACCCTGTTTGGTCAAAGTAG
CCTAGGGAAAAAACAAAACTGATGATGTTGCGTCCTCTAGAAAGAGCAGGCCTGGCTTTTGGTTCCCTCAGCA
TGAGTTTGAGGTCCTAGGCTATCCAGCCTATCACCGGCCTGTGGAATTGTCCTTTCAGCTCTCCCCTGGAGAAC
AGTCATGGGGATTCGACCCCCTGCAATGCTCGATTCCCCCTAGATCCTTTTATTGGCAGCCTGCCTATTACTGTT
CTGCTACTATTGCGCTAGCATTCAGAAAAAAAAAAGGGTCAGAAATCTAAATTACGTTCAAGCATTTTAGAGTT
CAAGTATTATC-3'

Reference sequence for NGS analysis

5'TCCTGTGTTAAGGGGTCCTTGAATCTTGAAGAATGGTTTGAGCCCCTGCTTTTGGACCCGGGGTTCCTCCATC
TAGGTCAATGGCTGTTTGGGGTGTTCCCTCTGCAGGAGACTACACGGACTTCTACAGCTCTCGGCAGCATGCC
ACCAATGTTGGCATTATGTTCAGAGGCAAGGAGAATGCGCTGTTGCCAAATTGGTATGTCCTAGACCAGATGC
TGGGATAAATTCAAAGTCGGCTCTTCTCTACAGTATGTTTTTCCCAGCAGCAAAGACCCTGTTTGGTCAAAGTA
GCCTAGGGAAAAAACAAAACTGATGATGTTGCGTCC-3'

Transparent Methods

Key Ressources Table

Reagent	Ressource	Identifier
Antibodies		
FAH Antibody	Abcam	ab81087
Vinculin Antibody	Abcam	ab73412
Anti-AAV VP1/VP2/VP3 mouse monoclonal supernatant, B1	Martin Müller, DKFZ, Heidelberg, Germany	N/A
Chemicals, Peptides and Recombinant Proteins		
VECTASTAIN® Elite® ABC HRP Kit (Peroxidase, Standard)	Vector Laboratories	Catalog #: PK-6100
2-(2-nitro-4-trifluoromethylbenzoyl)-1,3-cyclohexanedione (NTBC)	Sigma-Aldrich	PHR1731-1G
Target retrieval solution (Dako)	Agilent	Catalog #: S1699
Commercial Assays		
QuantiTect SYBR PCR Kit	Qiagen	Catalog #: 204141
AAV2 Titration ELISA 2.0R	Progen	Catalog #: PRAAV2R
AAV8 Titration ELISA		Catalog #: PRAAV8
TURBO™ DNase	Invitrogen	Catalog #: AM2238
DecaLabel DNA Labeling Kit	Thermo Fisher	Catalog #: K0622
KAPA real-time library preparation kit	KAPA Biosystems	Catalog #: KK8220
Experimental Models: Organisms/Strains		
C57BL/6 *Fah*$^{\Delta exon5}$		
Software and Algorithms		
Prism 5	Graphpad Inc	
Mfold	http://unafold.rna.albany.edu/?q=mfold/DNA-Folding-Form	(Zuker, 2003)
CRISPRESSO	http://crispresso.rocks/	(Pinello *et al.*, 2016)
ImageQuant TL v2003	Amersham Biosciences	

Contact for reagent and ressource sharing

Further information and requests for resources and reagents should be directed to and will be fulfilled by the lead contact, Michael Ott (Ott-MHH@gmx.de) and Hildegard Büning (buening.hildegard@mh-hannover.de).

Method Details

Animals

Eight- to 20-weeks-old C57BL/6 FahΔexon5male and female mice were used for all studies(Grompe et al., 1993). The animals were maintained on a regular day and night cycle and continuously supplied with 2-(2-nitro-4-trifluoromethylbenzoyl)-1,3-cyclohexanedione (NTBC) in the drinking water until the time of experimentation or when indicated. In general, NTBC was added for two to four days in case of weight loss below 80% of the original weight at the start of the experiments. Occasional NTBC treatment occurred up to four weeks after cell transplantation or vector administration. Before and after surgical interventions metamizol was administered via drinking water. Interventions were performed during daytime-.For determination of initial repair rates, NTBC supplementation was continued until the end of the experiment. Appropriate negative control experiments were conducted with sibling littermates. Mouse embryonic fibroblasts (MEF) were isolated from day 13.5 p.c. embryos according to standard protocols (Durkin et al., 2013). Animal handling and experiments were performed according to the guidelines of the Hannover Medical School, Hannover, Germany, and with permission of the local authorities (TVA 17/2658).

Guide RNA design

Targeted *S. aureus* Cas9 gRNAs were selected by screening the Fah exon 5/neoR junction for the protospacer adjacent motif (PAM) NNGRRT. The 23 nucleotides 5’ of this motif were selected and equipped with a 5’ leading G, when required.

Cloning of vector constructs

The single-stranded AAV vector coding for the LP1 promoter-driven *S. aureus* Cas9 followed by the bovine growth hormone (bGH) poly(A) and is referred to pSSV9-LP1-SaCas9. A second vector encoding the Fah donor template was generated using the

AAV TRISPR cloning system, which relies on two consecutive steps of Golden Gate Assembly. Details of this system and of the cloning steps will be reported elsewhere (manuscript in preparation). Briefly, oligonucleotide pairs P20/P21 and P22/P23 encoding gRNAs (Supplemental Table 1) were first cloned into donor plasmids conferring resistance to chloramphenicol, followed by concatenation of multiple gRNA-encoding cassettes from individual donor plasmids along with the Fah repair template into a single self-complementary AAV recipient plasmid comprising the viral ITRs of serotype 2. Next, plasmid DNA from individual clones was extracted, and the gRNA sequence validated by Sanger sequencing. In a consecutive Golden Gate Assembly step, two donor plasmids - one encoding gRNA1 (targeting the 5' region of the neoR sequence) under transcriptional control of the human U6 promoter, the other encoding gRNA2 (targeting the 3′ region of the neoR sequence) under transcriptional control of the 7SK promoter - as well as the gBlock_FAH_repair_Template (Table 6) and the AAV recipient plasmid from the AAV TRISPR toolbox were subjected to another Golden Gate Assembly reaction. The resulting plasmid was digested with AgeI/SalI to remove a YFP (yellow fluorescent protein) stuffer sequence present in the parental AAV TRISPR plasmid for replacement with annealed oligonucleotides GGC-Lock_AgeI/SalI_fw/GGC-Lock_HindIII/Sal_MCS_rv, yielding the final vector AAV-DV-donor-2gRNAs. Based on this vector, the AIO-SL vector was constructed as described below.

The AIO-SL construct was generated via three overlap extension PCRs and a subsequent cloning step. The donor template was flanked with the original genomic target sequences including PAMs via PCR using primers P1 and P2. U6 and 7SK promoter-driven gRNA cassettes were amplified using primer pairs P3/P4 and P5/P6. In a third PCR using primers P3 and P6, the donor template was fused to both gRNA expression cassettes. This final PCR product was digested with NotI and KpnI and subsequently ligated into pSSV9(Samulski, Chang and Shenk, 1987) carrying LP1-SaCas9(F. Ann Ran, Le Cong and Winston X. Yan, 2015). The AIO-NL construct was generated by the same strategy using P32 and P33 for donor template amplification. U6 and 7SK driven gRNA cassettes were amplified using P3/P30 and P5/P31.

The four SpCas9-encoding AAV vectors utilized for the oversized genome packaging experiments in Figure 6d-e are described in (Fakhiri *et al.*, 2019).

AAV production

For production of the VP2-deleted AAV2, the VP2 start codon within the cap open reading frame (ORF) in the AAV2 helper plasmid pRC(Girod et al., 1999) was modified (ACG to ACC) by site-directed mutagenesis as described previosly(Lux et al., 2005), resulting in plasmid pRCVP2k.o. Using the same strategy, pXR-8VP2k.o. was cloned using pXR-8 (kindly provided by James Wilson, University of Pennsylvania, PA, USA) as basis. In both constructs, expression of AAV2 Rep proteins and the serotype-specific VP1 and VP3 capsid proteins remained unchanged. For production of VP2-deleted AAV vectors, HEK293 cells were seeded at 80% confluency and triple-transfected with the vector plasmid (AIO-SL.AAV or AIO-NL.AAV), the AAV helper plasmid pRCVP2k.o. or pXR-8VP2k.o. and the adenoviral helper plasmid pXX6-80(Xiao, Li and Samulski, 1998) (kindly provided by Jude Samulski, University of North Carolina at Chapel Hill, NC, USA) at a 1:1:1 molar ratio. Forty-eight hours post-transfection, cells were harvested, pelleted by low-speed centrifugation and lysed. Vectors were purified from cell lysates by iodixanol step gradient as described previously(Lux et al., 2005). Genomic particle titers were determined by quantitative (q)PCR following isolation of vector genomes (DNeasy Blood & Tissue kit, Qiagen) using specific primers listed below. Capsid titer was determined by AAV2 and AAV8 specific ELISA (Progen). For comprehensive analysis of vector genome packaging capacity, AAV2, AAV2$^{\Delta VP2}$, AAV8 and AAV8$^{\Delta VP2}$ were produced in parallel as described above and purified by continuous CsCl gradient as described previously(Bernaud *et al.*, 2018). Indicated fractions were collected, DNA was isolated (DNeasy Blood & Tissue kit, Qiagen) and analyzed by Southern blotting.

Engineering of directly reprogrammed hepatocytes from C57BL/6 Fah∆exon5 embryonic fibroblasts

Directly programmed hepatocytes (iHeps) were generated as previously published(Song et al., 2016). Briefly, 1x10^5 primary MEF were transduced with a lentiviral vector encoding HNF1, GATA4, FOXA3 and HNF4 at a multiplicity of infection (MOI) of 5 as follows. One day after transduction, complete DMEM medium was replaced by HCM Hepatocyte Medium (Lonza). Cells were maintained in HCM medium, with medium changes every other day. On day 14 after transduction, the cells were tested for albumin and α1-antitrypsin protein secretion as well as

Cytochrome P450 (CYP) activity, or harvested for mRNA isolation and RNA-Seq analysis.

Ex vivo gene correction of Fah deficiency

Fah-deficient iHeps were transduced with AIO-SL.AAV2□VP2 at a MOI of 5×105. Fourteen days post-vector application, cells were analyzed via qPCR, NGS or histological staining.

In vivo gene correction of Fah deficiency

A number of 5×1010 AIO-SL.AAV8$^{\Delta VP2}$ particles was diluted in 50 µl 0.9% saline solution and injected into the tail vein of C57BL/6 Fah∆exon5 mice. On the day of vector injection, NTBC was withdrawn from the drinking water to facilitate repopulation of the recipient liver by gene-corrected cells.

Quantitative real-time (qRT-) PCR

To determine the ratio between genomes that had retained the neoR sequence and those lacking it, genomic DNA was analyzed via qRT-PCR using the QuantiTect SYBR PCR Kit (Qiagen) and a GAPDH-specific primer pair (P9/P10) as well as one detecting neoR (P7/P8), both annealed at 60°C. Quantitative RT-PCR was performed in a Mx3005p cycler (Stratagene) with at least three technical replicates of each sample. The relative difference in number of neoR copies was determined by normalization to an untreated control. Differences of the Ct-values were calculated using the 2-ΔΔCT method(Livak and Schmittgen, 2001). Integrety of vector genomes was determined using three amplicons generated by PCR using primers P24/P25, P26/P27 and P28/P29 as indicated in figure 2a (green lines).

Reverse transcription quantitative PCR (RT-qPCR)

RNA from liver tissue was isolated using RNAzol® according to the manufacturer's protocol. Prior to cDNA synthesis and quantitative real-time PCR using QuantiTect SYBR® Green PCR Kit (Qiagen), total RNA was treated with TURBO™ DNase (Invitrogen) for 15 minutes at 37°C. Fah mRNA was detected using primers P18/P19. Ct-values were analyzed using the $2^{-\Delta\Delta CT}$ method.

Next-generation sequencing

The ~1 kb PCR product generated by primers P11/P12 was purified and either subcloned into pMiniT vector (NEB) for single-amplicon sequencing or employed in a PCR using primers P11/P17 for next-generation sequencing (NGS) analysis . To avoid bias by over-amplification, library preparation was performed using the KAPA real-time library preparation kit (KAPA Biosystems). Libraries were sequenced on a MiSeq Sequencer (Illumina) using MiSeq Reagent Kit v3 (Illumina) to generate 2×300 base paired-end reads. Reads were mapped to reference (Supplemental Table 6) and variants identified by using the low-frequency variant detector function in CLC genomics Workbench v10 (https://www.qiagenbioinformatics.com/). Analysis of NGS data for homology-directed repair was accomplished using CRISPResso(Pinello et al., 2016).

Detection of genome editing and T7 endonuclease assay

To assess the efficiency of each gRNA, Fah-deficient MEF were seeded in gelatin-coated 6-well plates and transfected with 1 µg of CMV_SaCas9 and 1 µg of gRNA plasmid using 3 µl Lipofectamine LTX (Thermo Fisher Scientific). Genomic DNA was prepared three days post-transfection using the DNeasy Blood & Tissue Kit (Qiagen). The two targeted loci were amplified with primer pairs P13/P15 and P14/P12 using Q5 High-Fidelity DNA Polymerase (NEB). Next, the corresponding PCR products were purified using the QIAquick gel extraction kit (Qiagen) and 200 ng of the product were subjected to a T7 endonuclease I assay (NEB) according to the manufacturer's protocol. Reaction products were separated on a 1% agarose gel. To validate excision of the neoR sequence, genomic DNA of treated cells was isolated and subjected to PCR using primers P11, P12 or P16. Since primer P12 can only bind within the genome, it avoids false-positive PCR products generated from the donor template. This PCR generates two products, namely a ~2 kb fragment in the case of neoR retention and a ~1 kb fragment in the case of neoR removal.

Cell transplantations

Cells were harvested by trypsinization and centrifuged at low speed. Next, 1×106 cells were resuspended in 100 µl DMEM and injected into the spleen of C57BL/6 FahΔexon5 mice. On the day of transplantation, NTBC was withdrawn from the drinking water to facilitate repopulation of the recipient liver by gene-corrected cells. Cell-transplanted animals received NTBC for a period of two to four days during the 4

weeks after transplantation in case their body weight dropped below 80% of the original weight and were followed for up to seven months. Control animals that were injected with media only did not receive NTBC at any time point.

Immunocytochemical and immunohistochemical stainings

Liver tissues were fixed with 4% formalin, embedded in paraffin and cut into 5-µm-thick sections for histological and immunohistochemical analysis. After the deparaffinization and blocking procedure, the slides were incubated in target retrieval solution (Dako) at 98°C for 20 minutes. For FAH (primary antibody, Abcam, ab81087) staining, tissues were blocked with the Avidin/Biotin blocking kit (Vector laboratories). Biotinylated goat anti-rabbit and rabbit anti-goat antibodies (Vectastain, Vector laboratories) were used as secondary antibodies. Counterstaining was performed using hematoxylin (Merck Millipore).

Immunoblotting

For the detection of FAH protein, tissue was lysed using 1× sodium dodecyl sulfate (SDS) protein lysis buffer (62.5mM Tris-HCl [pH6.8], 2% [wt/vol] SDS, 10% glycerol, 50 mM dithiothreitol, 0.01% [wt/vol] bromophenol blue) and incubated at 98°C for 5 minutes. FAH (primary antibody, Abcam ab81087) was employed in a dilution of 1:500. Vinculin protein expression was detected using Vinculin antibody (ab73412, Abcam) in a dilution of 1:3000. For the detection of VP1, VP2 and VP3, anti-AAV VP1/VP2/VP3 mouse monoclonal supernatant, B1 (kindly provided by Martin Müller, DKFZ, Heidelberg, Germany) was employed in a dilution of 1:10. Detection was performed via the Odyssey infrared imaging system.

Southern blotting

Recombinant AAV genomes were obtained from purified AAV particles upon benzonase and proteinase K treatment. Next, isolated DNA suspension or GeneRuler Plus DNA ladder (Fermentas) were mixed with sodium hydroxide (NaOH) to obtain a final concentration of 0.1 M NaOH and incubated at room temperature for 5 minutes. Next, 100 or 200ng of DNA was loaded onto a 0.7 or 1% (50 mM NaOH, 1 mM EDTA) agarose gel and run at 30 Volts for 20 hours followed by Southern blotting as previously described(Sambrook and Russell, 2006). Using 20× saline-sodium citrate (SSC) buffer, DNA was blotted onto a nylon membrane and UV-

crosslinked. Next, 100ng SaCas9-specific DNA-probe (BamHI digestion of the AIO-SL plasmid) or SpCas9 specific DNA-probe (BamHI/NheI digestion of DH-003 kindly provided by Dirk Heckl, Hannover Medical School) were radiolabeled using DecaLabel DNA Labeling Kit (Thermo Fisher) and incubated with the membrane at 42°C over night. Vector-specific bands were detected using autoradiography .

Quantification and statistical analysis

Statistical analysis was performed using Graph Pad Prism v5. Mean value and standard deviation of biological and/or technical repliactes are indicated in the graphs. Signficicant differences were determined using standard two-sample Student's t-test. A p-value < 0.05 is indicated by an asterisk.